SUPERBURSTS: INVESTIGATION OF ABNORMAL PAROXYSMAL BURSTING ACTIVITY IN NERVE CELL NETWORKS IN VITRO

Nikita Suri, B.A.

Thesis Prepared for the Degree of

MASTER OF SCIENCE

UNIVERSITY OF NORTH TEXAS

May 2018

APPROVED:

Guenter Gross, Major Professor
Jannon Fuchs, Committee Member
Kamakshi Gopal, Committee Member
Art Goven, Chair of the Department of Biological Sciences
Su Gao, Dean of the College of Science
Victor Prybutok, Dean of the Toulouse Graduate School

Suri, Nikita. *Superbursts: Investigation of Abnormal Paroxysmal Bursting Activity in Nerve Cell Networks in vitro*. Master of Science (Biology), May 2018, 53 pp., 5 tables, 30 figures, references, 28 titles.

Superbursts (SBs) are large, seemingly spontaneous activity fluctuations often encountered in high density neural networks in vitro. Little effort has been put forth to define and analyze SBs which are paroxysmal bursting discharges. Through qualitative and quantitative means, I have described specific occurrences of superbursting activity. A complex of paroxysmal bursting has been termed a “superburst episode,” and each individual SB is a “superburst event” which is comprises a fine burst structure. Quantitative calculations (employing overall spike summations and coefficient of variation (CV) calculations), reveal three distinct phases. Phase 1 is a “build up” phase of increasingly strong, coordinated bursting with an average of a 17.6% ± 13.7 increase in activity from reference. Phase 2, the “paroxysmal” phase, is comprised of massive coordinated bursting with high frequency spike content. Individual spike activity increases by 52.9% ± 14.6. Phase 3 is a “recovery phase” of lower coordination and an average of a 50.1% ± 35.6 decrease in spike production from reference. SBs can be induced and terminated by physical manipulation of the medium. Using a peristaltic pump with a flow rate of 0.4ml/min, superbursting activity ceases approximately 28.3 min after the introduction of flow. Alternatively, upon cessation of medium flow superbursting activity reemerges after approximately 8.5 min. Additionally, this study explored other methods capable of inducing superbursting activity using osmotic shocks. The induction and termination of SBs demonstrates that the cell culture environment plays a major role in generating this phenomenon. The observations that

high density multi-layer neuronal networks in culture are more likely to enter paroxysmal bursting also supports the hypothesis that enrichment and depletion layers of metabolites and ionic species are involved in such unusual activity. The dynamic similarity of the SB phenomenon with epileptiform discharges make further quantification on the spike pattern level pertinent and important.

ACKNOWLEDGMENTS

This research was performed at the Center of Network Neuroscience (CNNS) at the University of North Texas (UNT). Critical private financial support was provided by Dr. Joseph Pancrazio, Carole and Jay Ross, Barbara Evans, Steven Gum, and PTAC Direct Sales. Special thanks to Harvey Wiggins of Plexon Inc. for equipment donation and repair.

I express my sincerest appreciation to fellow M.S. student, Edmond Rogers, for his support and his diligence in maintaining the laboratory. Further, I offer my gratitude to M.S. student, Stormy Durant, and undergraduate volunteers, Ross Hicks, Austin Moore, and Karan Bhakta for their reliable cell culture support. For the in-house fabrication of MEAs, I thank Ahmet Ors, Christopher Pino, and Jake Gray.

Thank you to the faculty of the University of North Texas Department of Biological Science for their immense support of my research; and above all, I owe my highest praise to the support of Dr. Guenter W. Gross for granting me this opportunity; his generous encouragement and direct involvement in this research was instrumental to my growth and success.

Finally, to Mom, Dad, and Pri: Thank you for being such an incredible part of my life; without your support, this would not have been possible.

TABLE OF CONTENTS

Page

LIST OF TABLES

Page

LIST OF FIGURES

Page

CHAPTER 1

INTRODUCTION

Neural networks grown on micro electrode arrays (MEAs) provide a unique platform for investigating neuronal function and are applicable to many areas of research. Regular native network bursting activity is characterized by clusters of high frequency action potentials separated by periods of inactivity. Superbursts (SBs) represent high-intensity burst oscillations which can last for a variable period of time. Superbursting activity can occur spontaneously under normal life support conditions with no external stimulation. Observations of spontaneous superbursting activity have been made over many years (Chiappalone et al., 2007; Gladkov et al., 2018; Kim et al., 2014; Krahe et al., 2004; Kowalski et al., 1992; Madhavan et al., 2007). The occurrence of SBs has an increased likelihood of appearance within higher density cultures, as higher amounts of cells within a network have been correlated with an increased risk of network instability (Idelson et al., 2010). The term “superburst” was coined in the 2006 thesis of Daniel Waagenaar, where he also linked this type of instability to highly dense networks (Waagenar, 2006). However, a quantitative description was not attempted and no other laboratory has yet tried to define this complex instability. The superbursting activity is epileptiform in nature and may be related to mechanisms of epilepsy. However, many experiments do show sudden paroxysmal bursting, which interferes with the quantification of experiments that depend on level plateau values. The latter is demonstrated with Fig. 1 where the titration of linopirdine depends on well-defined plateaus established after each addition of the test compound. Utilizing nerve cell dynamics for pharmacology requires stable reference activity as well as stable activity

plateaus from sequential applications of test substances, so that all activity changes can be related quantitatively to this native activity for each network (Fig. 1). Although each network has different initial activity, normalization in terms of percent changes from reference has proved to be a very effective method for comparing responses from different networks. Further, SBs make a network unsuitable for pharmacological application because of unexplained instability. Whereas Waagenar and Potter linked such activity to inherent network properties (Waagenar, 2005), more careful observations seem to indicate that life support conditions and possible cell density of the culture may be linked to the development of such instability (Segev et al., 2003). This implies that, under certain conditions, biochemical and physical-chemical factors affect the behavior of networks much more than inherent structural or cell population variations.

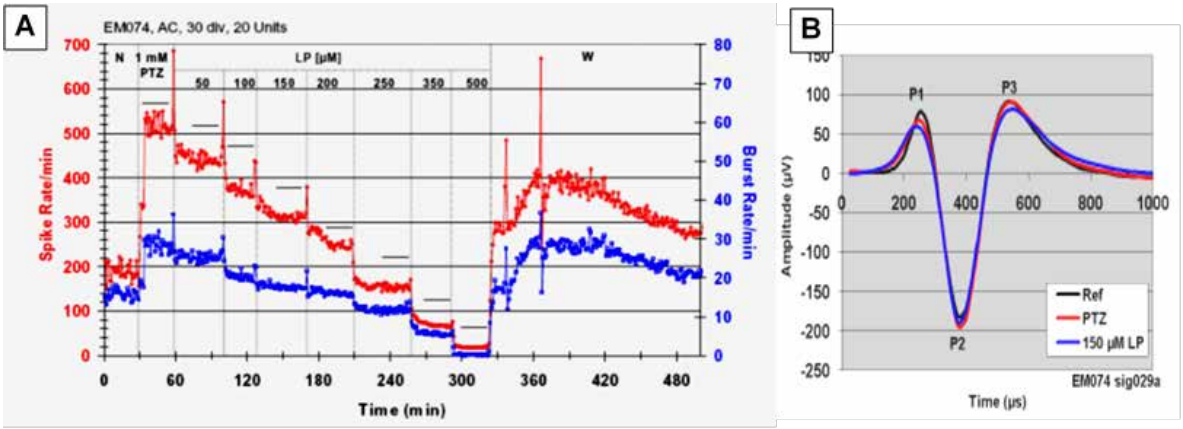

Fig. 1. Titration of a pentylenetetrazol-induced excited state (1 mM) with linopirdine followed by a single medium change (W). Normalization via percent decreases from the PTZ reference generates dose response curves and IC_{50} values used for compound characterization. Simultaneous waveshape data reveals effects on ion channels. From Wu et al., 2011 with permission.

Under normal conditions, networks show high activity stability over long periods of time. This stability is illustrated in Fig. 2, with consistency in number of channels (top

trace) and average spike rate (per min; bottom trace). The initial three activity changes were caused by pharmacological manipulation (stryrene applications). Stability has been maintained for several days (Gross et al, 2018) but is dependent on stable life support conditions.

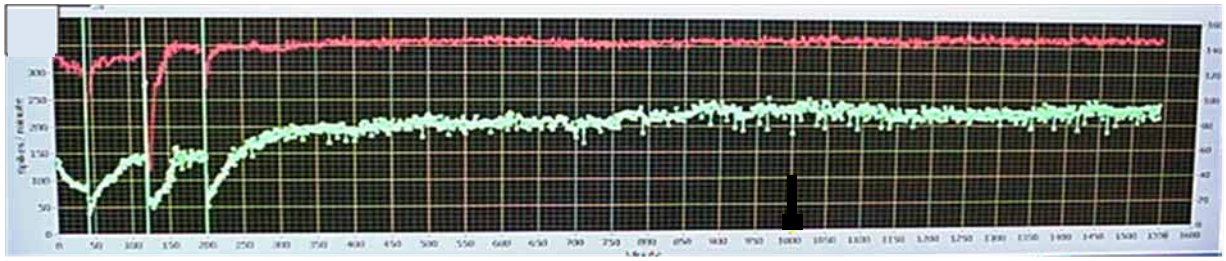

Fig. 2. Stability of network activity for 25 hrs after 3 pharmacological tests during the first 200 minutes. No major instabilities are observed (from Gross et al, 2018 with permission).

An example of intense bursting instability is shown in Fig. 3. Under such circumstances a quantitative description of pharmacological responses is difficult and often impossible. Each vertical “excursion” represents an almost doubling of spike rates for about one minute. The purpose of this thesis is to characterize the basic features of such activity and attempt to find its cause.

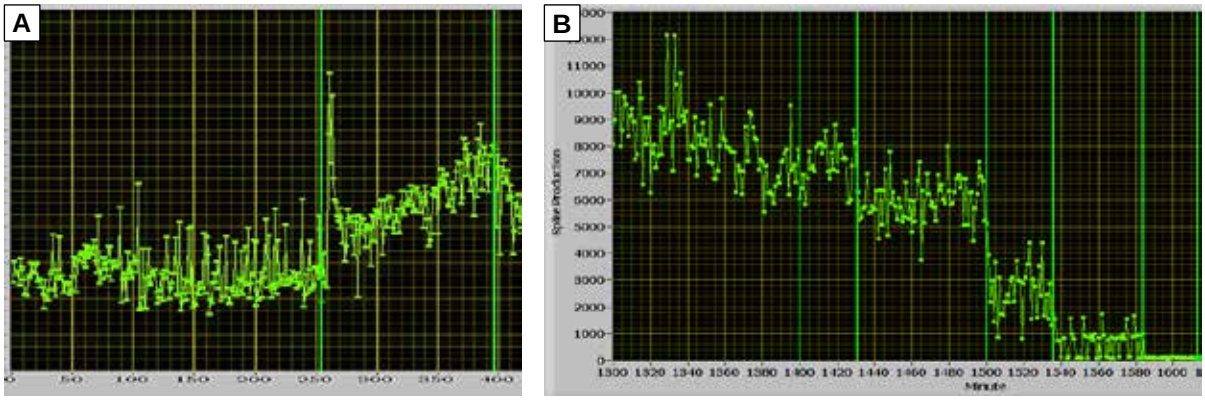

Fig. 3. Large fluctuations in network spiking activity. **(A & B)** Large vertical excursions indicate significant increases in total network spiking activity, varying considerably minute by minute. The vertical lines indicate the addition of a pharmacological substance.

In addition to contributing to ongoing efforts to accurately categorize and define SBs, this thesis demonstrates how to control network superbursting instability with external factors. Manipulation of recording chamber medium flow is one external factor that is presented. Medium stagnation and medium flow have different effects on local pH, osmolarity, and biochemical gradients. This “medium stratification” is most pronounced in the narrow, cylindrical recording wells during equilibrium conditions. In addition, increased network cell density further amplifies this medium stratification phenomenon. In animals, equilibrium conditions are never achieved, as pulsations, tissue movement, gravitational vectors, and blood flow all participate in gentle (and sometimes not so gentle) mixing. Laboratory experiments, however, usually aim for equilibrium conditions which in this case help generate the stratification problem. This issue came to light during recording from 8 network chambers situated in an isolation glove box. Stable activity was disturbed not just by test substance and osmolarity compensation water additions, but also by merely touching the meniscus of the medium with pipettes. The standard recording chambers used by the Center for Network Neuroscience (CNNS) (Fig. 6 and 7) prevented the development of extreme equilibrium conditions via asymmetric heating, producing gentle thermal currents, and by a CO_2/airstream, designed to maintain pH, which also allows for gentle convection of medium. It should be noted that the mixing phenomenon described in standard recording chambers was fortuitous, and not a result of intelligent design.

CHAPTER 2

OBJECTIVE

The objective of this thesis serves to advance the understanding of superbursts (SBs) by demonstrating their experimental induction and termination, and examining, defining, and quantifying their structure.

2.1 Specific Aims

SA1: Use experimental data to categorize, define, and quantify the fine structure of SBs.

SA2: Investigate causes of superbursting and explore protocols of SB induction and termination.

(a) Osmotic shock

(b) Medium flow rates

2.2 Hypotheses

H1: SB instability has biochemical origins and is not a direct characteristic of the network structure.

H2: SB instability is caused by stratification of metabolic components in a thin fluid layer above and below the network. Metabolic stratification causes enrichment and depletion layers close to the cells. Neuroactive molecules of interest include: potassium ions, ammonium ions, glucose, and polyamines.

CHAPTER 3

METHODS

3.1 Fabrication and Preparation of Microelectrode Arrays

Microelectrode arrays (MEA) were fabricated in house at the Center for Network Neuroscience (CNNS) using the methods described (Gross et al., 1985; Gross, 2011).

3.2 Cell Culture

Cell culture procedures were performed according to the protocols of Ransom et al., with small modifications previously published (Ransom et al., 1977, Morefield, 2000; Keefer et al., 2001). For the past 30 years, this laboratory has used tissue from embryonic mice. Whole embryonic tissue from the frontal cortex was used to obtain a ratio of neuronal and non-neuronal cells in culture that is similar to the parent tissue. Many pharmacological experiments have demonstrated that cell lines cannot be used to represent the functions of the parent tissue.

Mouse frontal cortices were dissociated enzymatically and with trituration. The cells were pooled, seeded onto multi electrode arrays (MEAs), and incubated for ~21 days (Fig. 4). Enzymatic dissociation was achieved using a trypsin/DNAse solution contained in a 15 ml. centrifuge tube, placed into an incubator for ~20 min., and subsequently examined every 5 min. for digestion progress. Cells were then centrifuged and the supernatant was eliminated to remove DNAse and trypsin from the cell mass. Cell concentrations were adjusted to 500k cells per ml. using a hemocytometer.

Cultures were incubated at 38^{o}C with 10% CO_2 to maintain steady pH levels of 7.4. Medium changes were performed biweekly in order to remove any metabolic waste

products. Osmolarity was constantly monitored and maintained at ~320 mOsmoles.

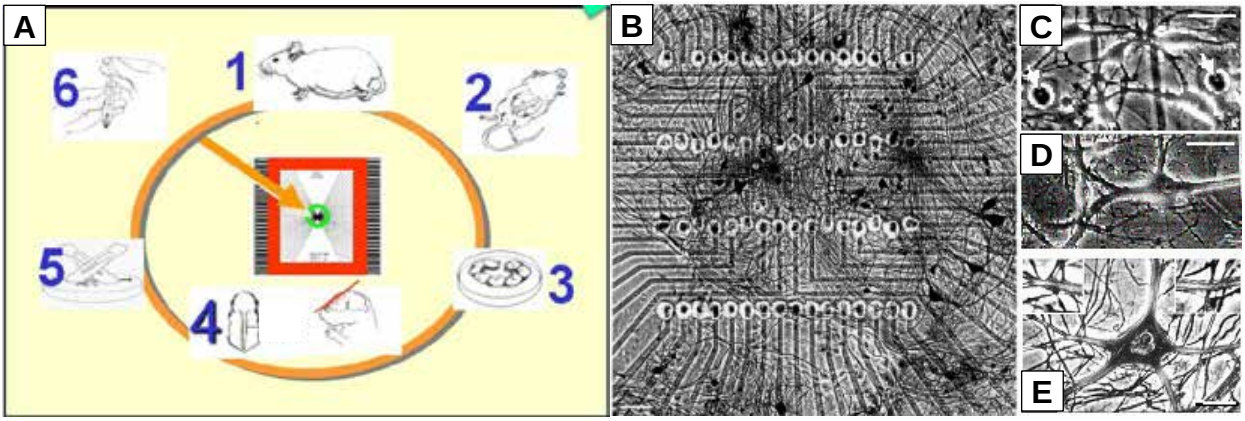

Fig. 4. Overview of cell culture procedure with an example of a neuronal circuits on MEAs. **(A)** Isolation and seeding of embryonic neural tissue from a time-pregnant mouse at E-16**.** Frontal cortices are isolated, dissociated, and seeded onto MEAs. **(B)** Fixed, Bodian stained mature spinal cord cells on an M-3 at 90 d.i.v. **(C & D)** Phase contrast micrographs of living neurons on an MEA. **(E)** Large interneuron stained with neurofilament antibodies (CNNS Archives).

3.3 Recording

Recordings were obtained from living neurons on MEAs coupled with a Plexon Multichannel Acquisition Processor (MAP) amplification and digitizing system (Plexon Inc., Dallas TX). System noise levels range from 30-40 microvolts, and large signal to noise ratios (Fig. 5) can be obtained with this platform. The array has 64 microelectrodes which are coupled to 64 channels in the Omniplex system. A special template matching algorithm (Plexon) monitors waveshapes that can yield up to four different discriminated units on a single electrode (see Fig. 5).

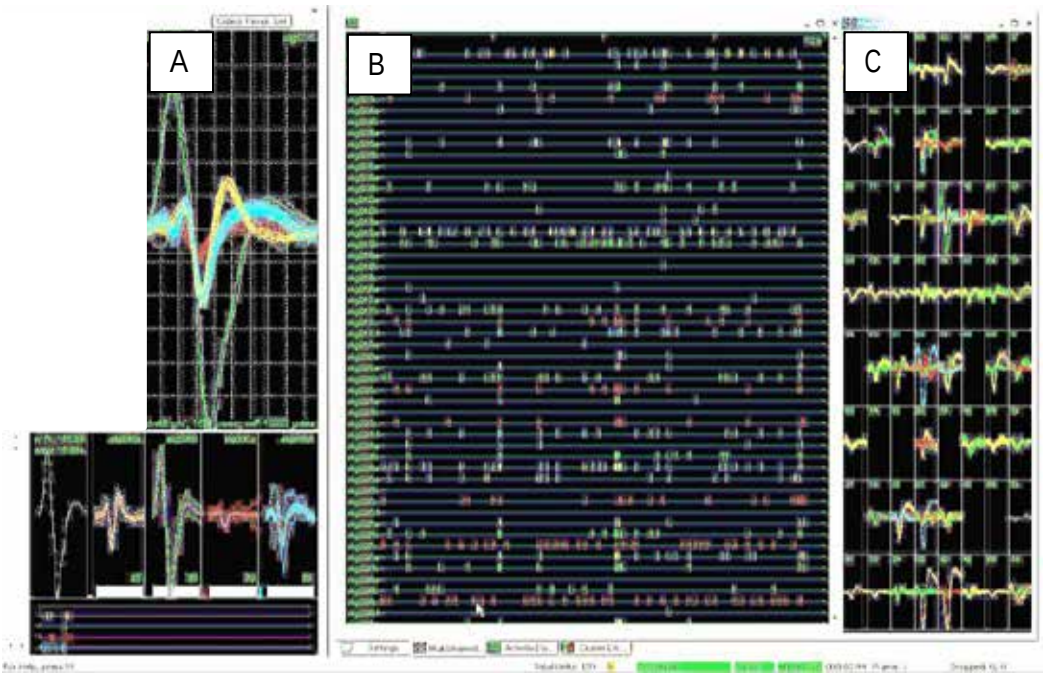

Fig. 5. Image of graphic user interface in Plexon software. **(A)** Four discriminated wave shapes isolated from a single electrode. **(B)** 2D raster display of time stamps. Each row represents a single discriminated unit. **(C)** Panels showing discriminated waveshapes from each electrode.

.

3.4 Chamber and Medium Flow

A modified life support system was combined with established recording methods (previous section) to obtain spontaneous culture activity (Fig. 6 and 7). This included the use of a peristaltic pump (Watson Marlow, 101U/R) to agitate medium in the culture chamber. Pre-discriminated action potential wave shapes and overall activity were monitored in real time and recorded for offline sorting with Plexon (Dallas, TX) software and additional programs designed in house.

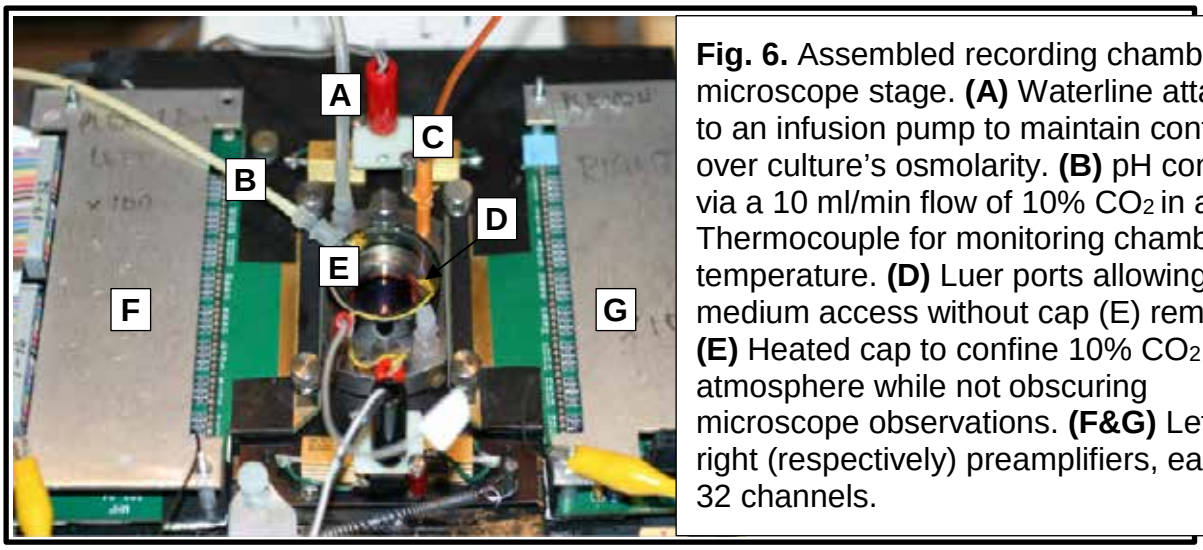

Fig. 6. Assembled recording chamber on microscope stage. **(A)** Waterline attached to an infusion pump to maintain control over culture's osmolarity. **(B)** pH control via a 10 ml/min flow of 10% CO_2 in air. **(C)** Thermocouple for monitoring chamber temperature. **(D)** Luer ports allowing medium access without cap (E) removal. **(E)** Heated cap to confine 10% CO_2 atmosphere while not obscuring microscope observations. **(F&G)** Left and right (respectively) preamplifiers, each with 32 channels.

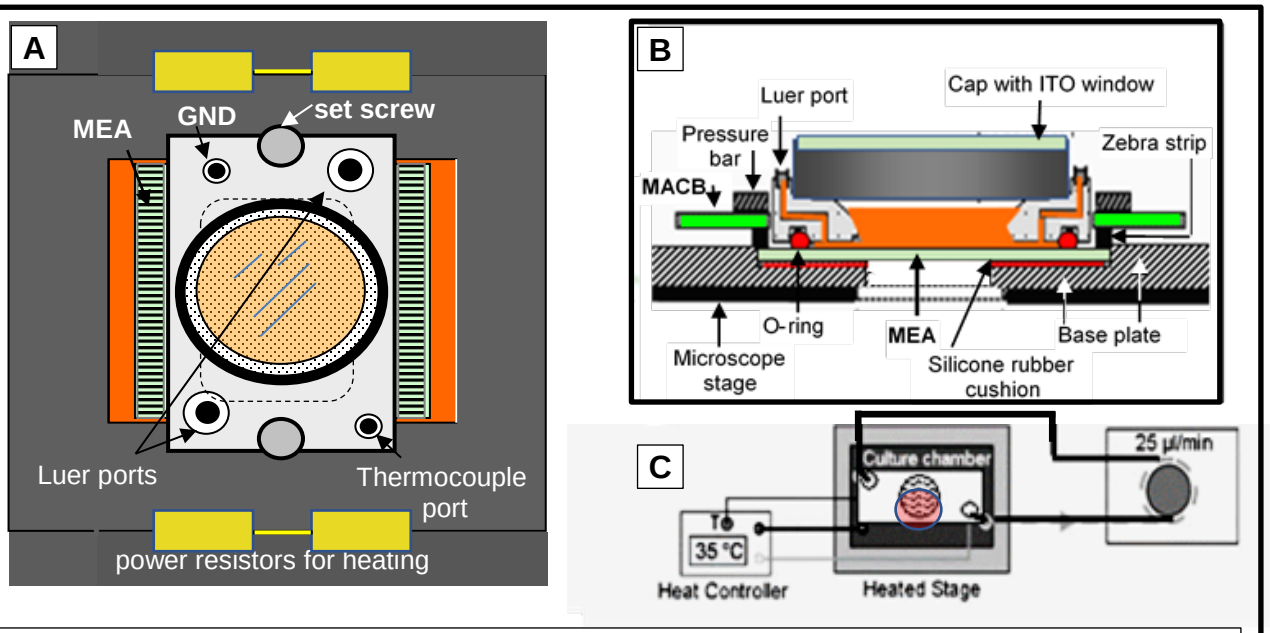

Fig. 7. Diagram of stainless steel chamber connected to base plate. **(A)** Overhead view; **(B)** Side view. **(C)** Diagram of peristaltic pump connected to chamber via Luer ports with temperature control (Gross and Schwalm, 1994; Meyer et al., 2009).

To prevent or reverse the hypothetical stratification thought to be responsible for superbursting, a gentle convection was introduced in the medium and network responses were observed. Convection was produced with a Watson Marlow peristaltic pump (Model: 101U/R) at various speed settings. The experimental chamber and pump set up is shown in Fig. 8.

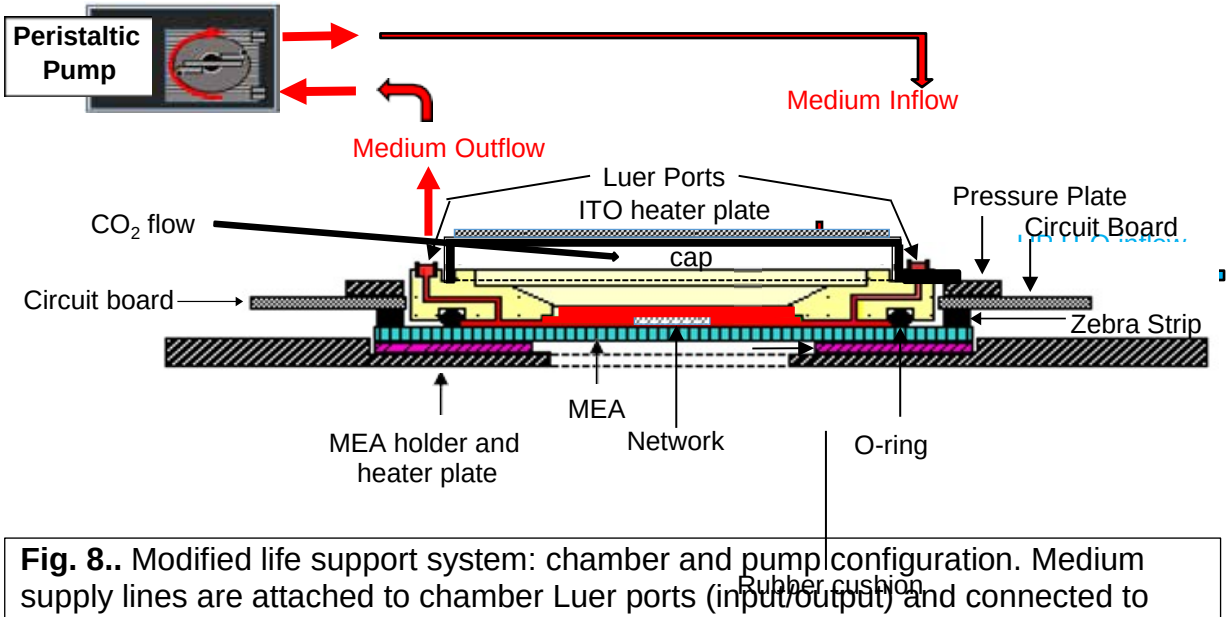

Fig. 8.. Modified life support system: chamber and pump configuration. Medium supply lines are attached to chamber Luer ports (input/output) and connected to a peristaltic pump (Watson Marlow 101U/R), generating a constant flow of medium. Luer port micro conduits exit into the O-ring domain inside the stainless-steel chamber. The ITO heater plate prevents condensation build up, allowing for continual morphological observation with a microscope. The pH is controlled with a 10 ml/min stream of 10% CO_2 in air injected into the cap. Water loss is compensated with an infusion pump. (Recording chamber: Gross and Schwalm, 1994).

Pharmed tubing was used to transfer medium through the pump system to maintain a relatively stable temperature, pH, and osmolarity level. In addition, a ~6mm. diameter “T” was attached to the chamber’s input Luer port when the peristaltic pump was utilized. This attachment allowed for the sterile addition of ultra-pure water via a syringe pump (Harvard Apparatus -Model 11 Plus) to maintain the osmolarity of the culture medium. This configuration maintained a constant osmolarity of ~320 mOsm.

3.5 Programs Utilized in Superburst Data Analysis

To analyze the paroxysmal superbursting phenomenon two programs, Vernac and Neuroexplorer were extensively utilized. Vernac is an in-house designed system from which minute by minute averages of active unit network spiking activity are computed. Active units are pre-discriminated waveshape forms isolated in Plexon (criterion: 10 threshold crossing of a wave-shape identified unit per minute). On the Vernac visual (Fig. 9), the red trace depicts the number of active channels, while each green dot depicts average network spiking activity occurring within one minute.

Neuroexplorer is a data analysis software program designed for neurophysiology by NeuroExplorer.com. By utilizing this software, isolated waveforms and resulting spiking activity from Plexon may be examined by utilizing a variety of other analyses (average spiking activity for specified bin sizes, summation of spiking activity, and oscillation frequencies).

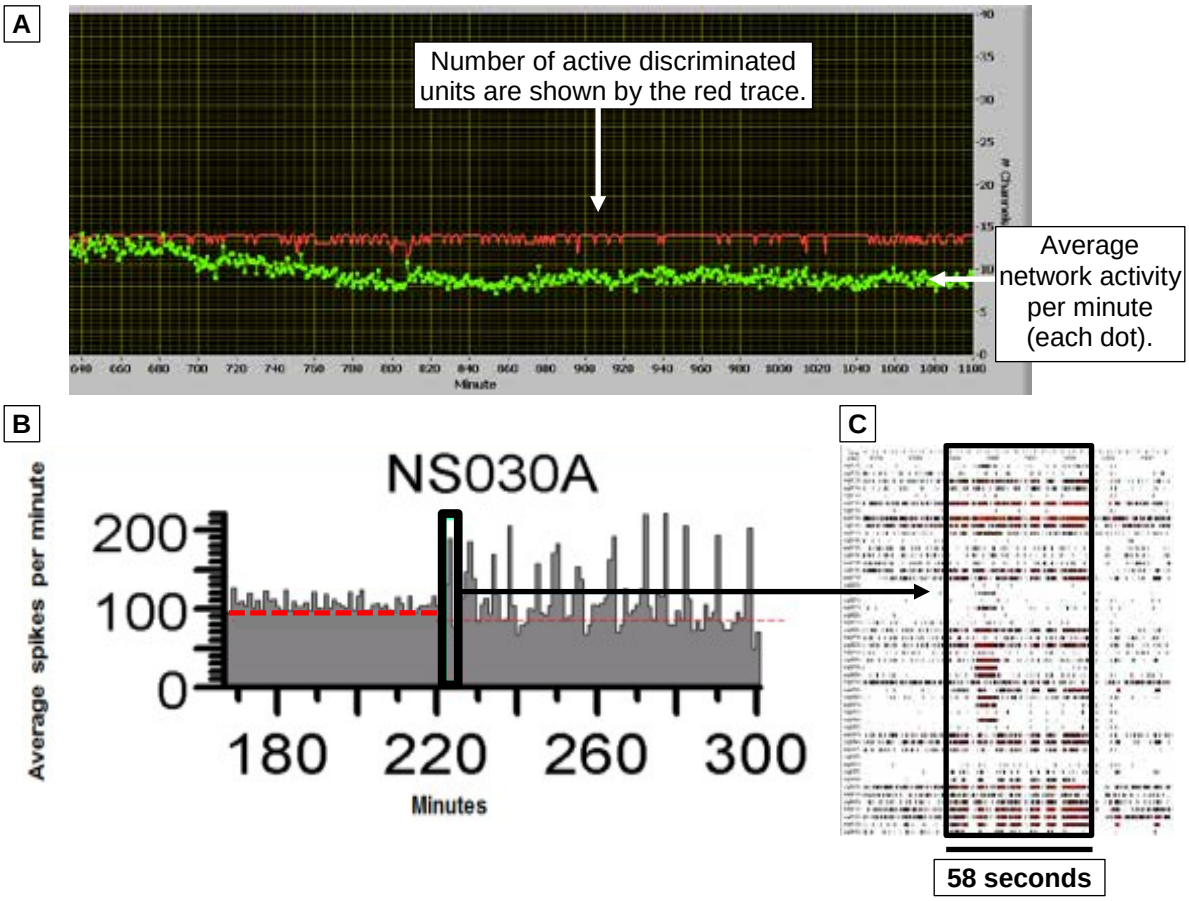

Fig. 9. Displays utilized in superburst data analysis (Vernac & Neuroexplorer). **(A)** Vernac display, which is utilized to visualize active unit and average network activity trends during experimental manipulations. The panel shows average network activity (green dots) from wave-shape discriminated neuronal signals (NS030A). The number of active units is shown by the red trace. An active unit is defined as any channel with 10 or more spikes detected per minute. This "floating average" is calculated for each minute. **(B)** Neuroexplorer (NEX) display of average spikes per minute is shown for comparison. The red line represents an average and the boxed region highlights 58 seconds of superbursting activity expanded in (C). **(C)** A raster plot depicting individual unit activity. Each tick mark represents an action potential threshold crossing (resolution 25 µs).

CHAPTER 4

RESULTS

4.1 Qualitative Analysis of SB Profiles

SBs are characteristically variable and therefore difficult to quantitatively define using standard measures. However, some basic terminology must be described to properly interpret these efforts.

4.1.1 SB Terminology

A “superburst event” (SB event) is a short (4.4 min ±1.2, n= 12) and sudden increase in average neuronal spike activity from reference (minimum: 50%). Multiple SB events are featured in Fig. 10, each with significant spike rate increases and peaks lasting no more than ~1 min. In addition, Fig. 10 also demonstrates a “superburst episode” (SB episode), which is an activity sequence comprised of multiple SB events. Detailed activity explanations are provided in subsequent sections.

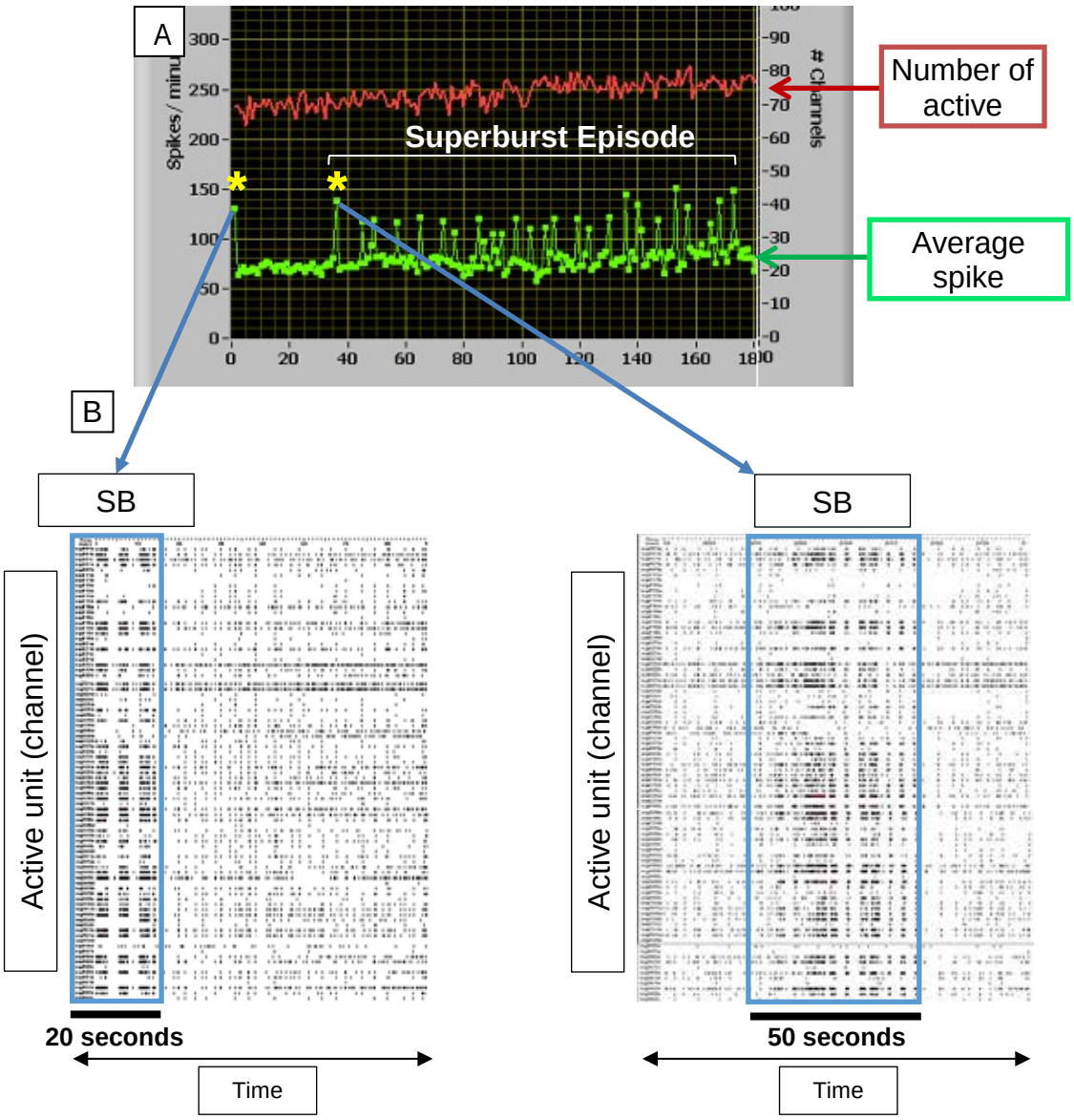

Fig. 10. Visual description of SB episode and events. **(A)** Spontaneous development of a SB episode comprised of multiple SB events. Individual SB events are characterized by a 30-100% increase in average spike rates. Number of discriminated units are shown by the top trace. It is interesting to note that the number of active units remains stable during paroxysmal superbursting activity. **(B)** Two raster plots depicting individual unit activity, where each tick mark represents an action potential threshold crossing (resolution 25 µs). The starred superbursts in (A) are further analyzed in (B) to show the complicated fine structure of bursting patterns that comprise each SB event.

4.1.2 General Description of SB Profiles

A SB episode is preceded by stable reference activity (Fig. 11). It is comprised of 12 individual SB events. Single data points (green dots, VernAC) represent 1 min. recording periods and contain activity fine structure (as shown in Fig. 10B) that will be further explained in section 4.2.2. Relative reference activity is defined as the stable period (>80 min.) immediately preceding the SB episode. An average of this reference activity is taken for the specified time period which is used to compare and quantify activity changes. Native state activity (activity immediately following chamber assembly) is referred to as absolute reference.

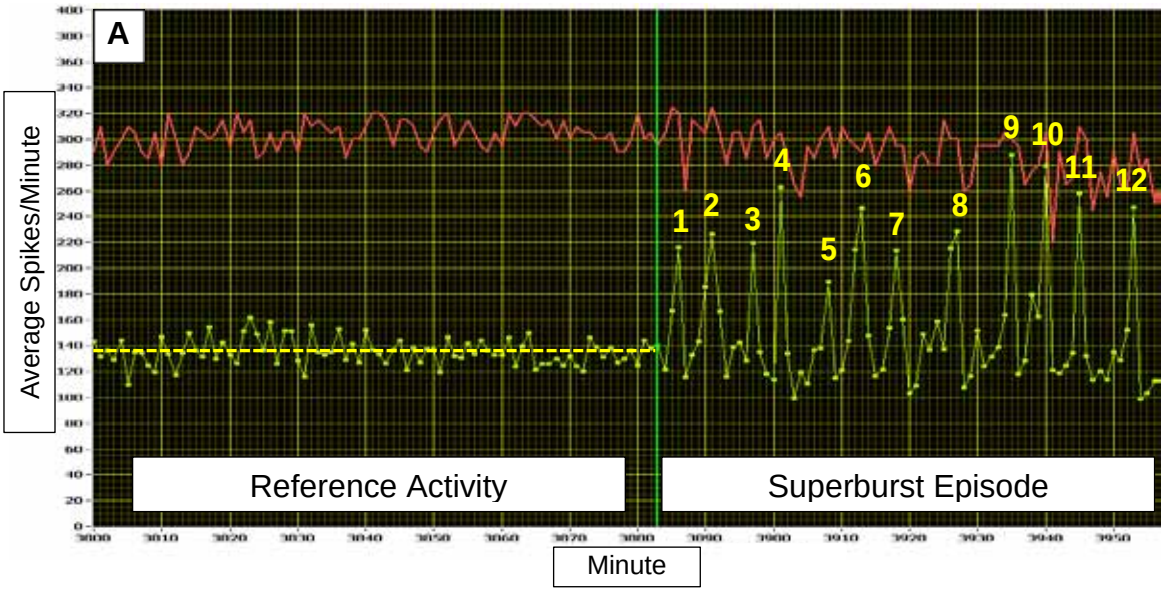

B

SB Event #	SB Event Duration (min)	Period (min)	Interval (min)
1	3	3	0
2	6	9	3
3	4	4	0
4	3	5	2
5	4	4	0
6	6	6	0
7	5	10	5
8	3	6	3
9	5	5	0
10	6	6	0
11	5	9	4
12	3	8	5
Avg	**4.4**	**6.3**	**1.8**
SD	**1.2**	**2.3**	**2.1**

C

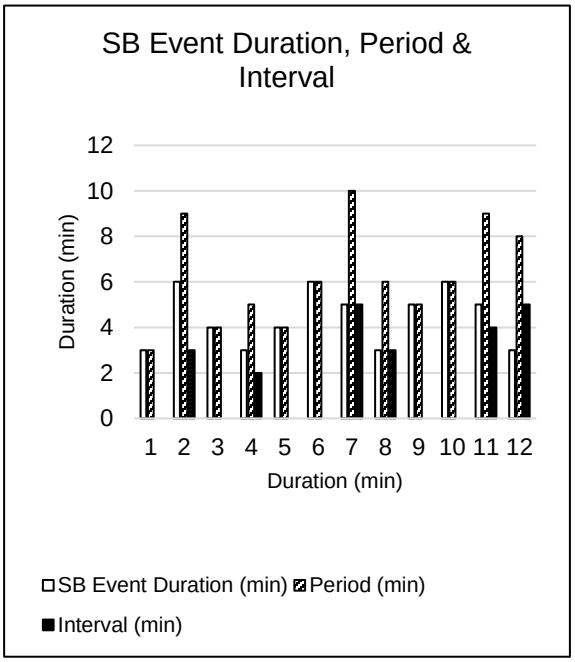

Fig. 11. General description of one SB episode. **(A)** Transition from stable activity to a SB episode. A SB episode is a phenomenon consisting of several individual SB events occurring over a period of time (~70min shown). **(B)** Counts of each individual SB duration, period (time between consecutive SB event beginnings), and interval (time between the end of one SB to the beginning of the next). Consecutive green dots (average activity per minute) that reach activity levels of at least 20% above the relative reference activity are counted and reported as the event's duration. Similar counts are performed to determine the SB period and interval. **(C)** A bar graph depicting information from (B).

4.1.3 Bin-Size Dependence of SB Profile Visualization

Dividing the range of values in question into a series of intervals creates “bins”. Multiple bin sizes can be utilized by the user to better visualize changes in network activity patterns (Fig. 12). Smaller bin sizes increase profile resolution and provide a more detailed depiction of network activity, while larger bin sizes allow for a general overview of changes. Each approach is valuable, and therefore bin sizes were adjusted with respect to the level of analysis being performed. However, infinitely decreasing and increasing bin size values inevitably results in the loss of clarity. With the exception of the explanation in Fig. 12, bin size parameters were consistently set as follows: SB episode, bin= 10- 60 sec; SB event, bin= 1 sec.

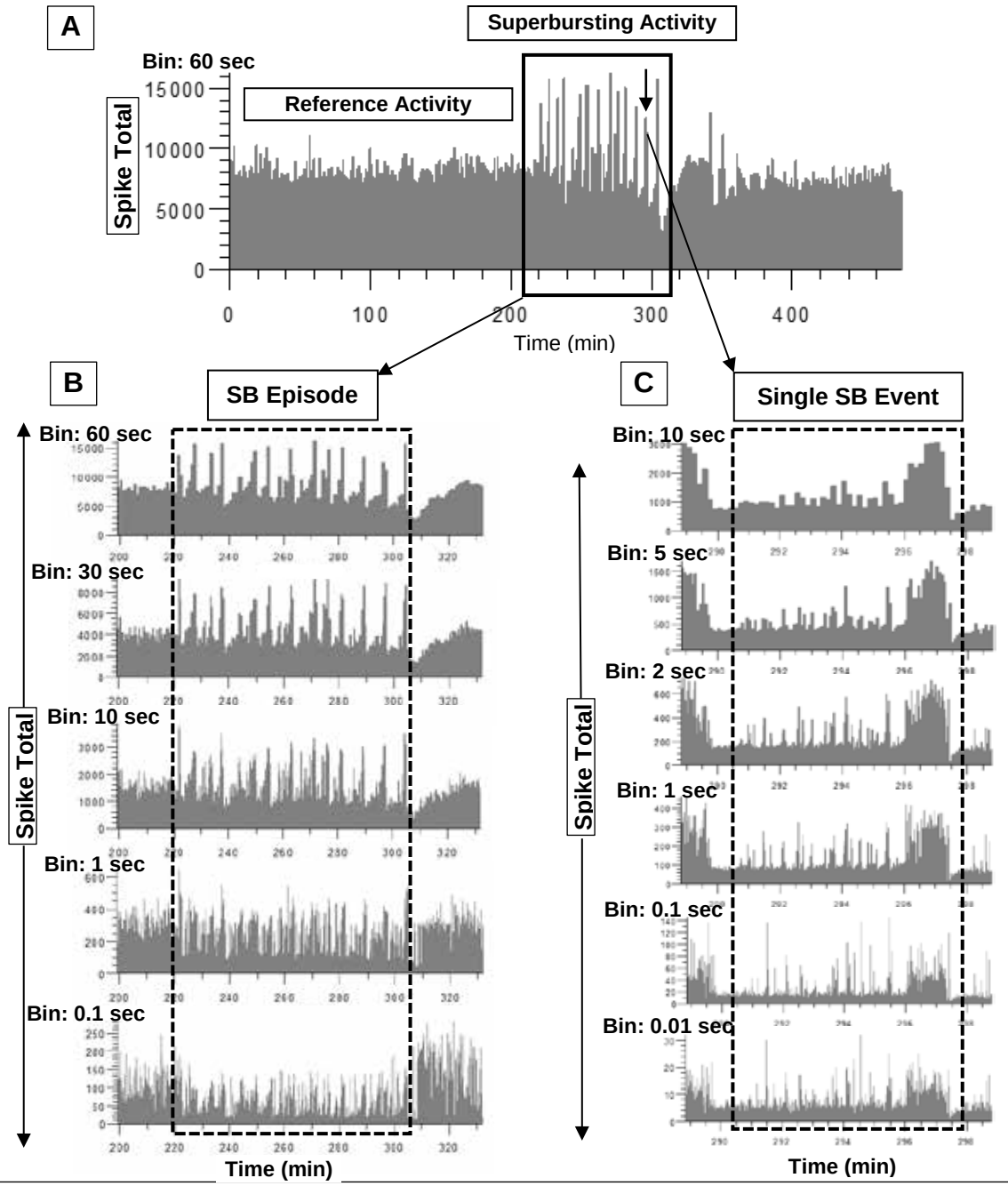

Fig. 12. Overview of bin sizes. Multiple spike density bin sizes reveal different features of an activity profile, with more details emerging as the bin becomes smaller. However, as a lower limit is approached, the pattern features disappear. **(A)** Overview of transition from reference to a SB Episode in a 480 min. segment. **(B)** SB episode (130 min.) enlarged and shown with decreasing (downward) bin sizes. 60 sec. bins depict general trends in spiking activity, while in 0.1 sec. bins disguise most spiking pattern features. All SB episode analyses were completed using 10 - 60 sec. bins. **(C)** Single SB event (~7 min.) also enlarged to illustrate decreasing (downward) bin sizes. As before 10 sec. bins are too large and feature only general trends, while 0.1-0.01 sec. bins are too complex for general analysis. All SB event fine burst structure analyses were completed using 1 sec. bins.

4.2 SB Profile Quantification

4.2.1 SB Average Activity and Total Spike Production

Real time average activity measurements (VernAC) provided a convenient method for viewing overall changes in network activity (Fig. 13). However, this broad approach obscured the fine structure of network activity needed to properly describe SBs. A greater level of detail was achieved using Neuroexplorer (NEX).

Fig. 13 shows a VernAC display and initial analysis. Green dots indicate the average spiking activity of a culture, or the number of spikes divided by active channels (average spikes per min). A channel is defined as “active” if it matches the unit’s template (“fires”) at least 10 times per minute. All VernAC displays show overall average network spiking activity. However, NEX is able to view of the sum of spikes occurring within a user defined bin size. This approach is slightly more refined than the floating average previously described and will be the main method used in further analysis. ~66 min. of corresponding VernAC and NEX displays for experiment NS030A are shown in Fig. 13 for comparison.

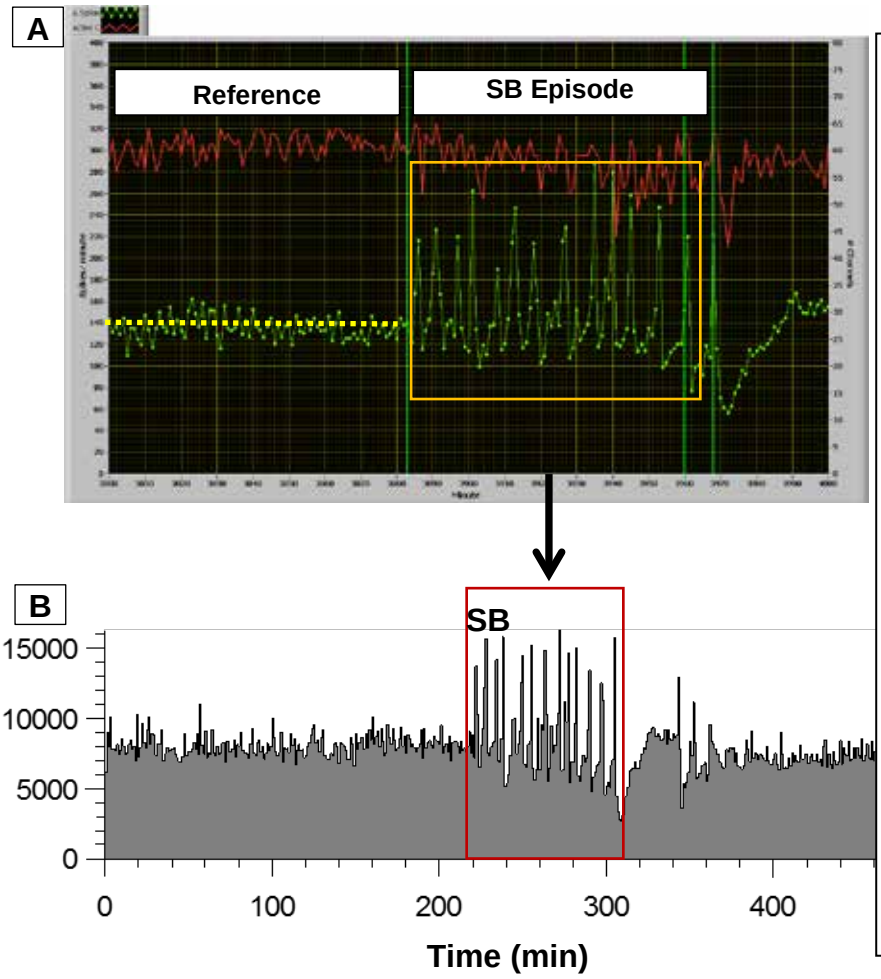

Fig. 13. SB Episode Comparison of VernAC (A) and NEX (B). **(A)** VernAC depiction of one SB Episode, comprised of multiple SB Events, lasting approximately 66 minutes. The bottom trace is the average activity, and the top trace is the number of active channels. **(B)** NEX (total spike production) depiction of same activity segment, using 60 sec. bins (equivalent to VernAC). Program differences result in unlike x-axis values, however, data segments are similar in length (200 min. and 480 min. respectively).

4.2.2 SB Fine Structure Analysis

With greater activity profile resolutions (decreasing bin sizes), increasingly complicated SB fine structure were revealed. Fig.14 isolates 1 of 4 SB events from 1 SB episode for further analysis with increased resolution. It is interesting to note that a pattern begins to emerge (“Introduction of Phases”, described in the next section).

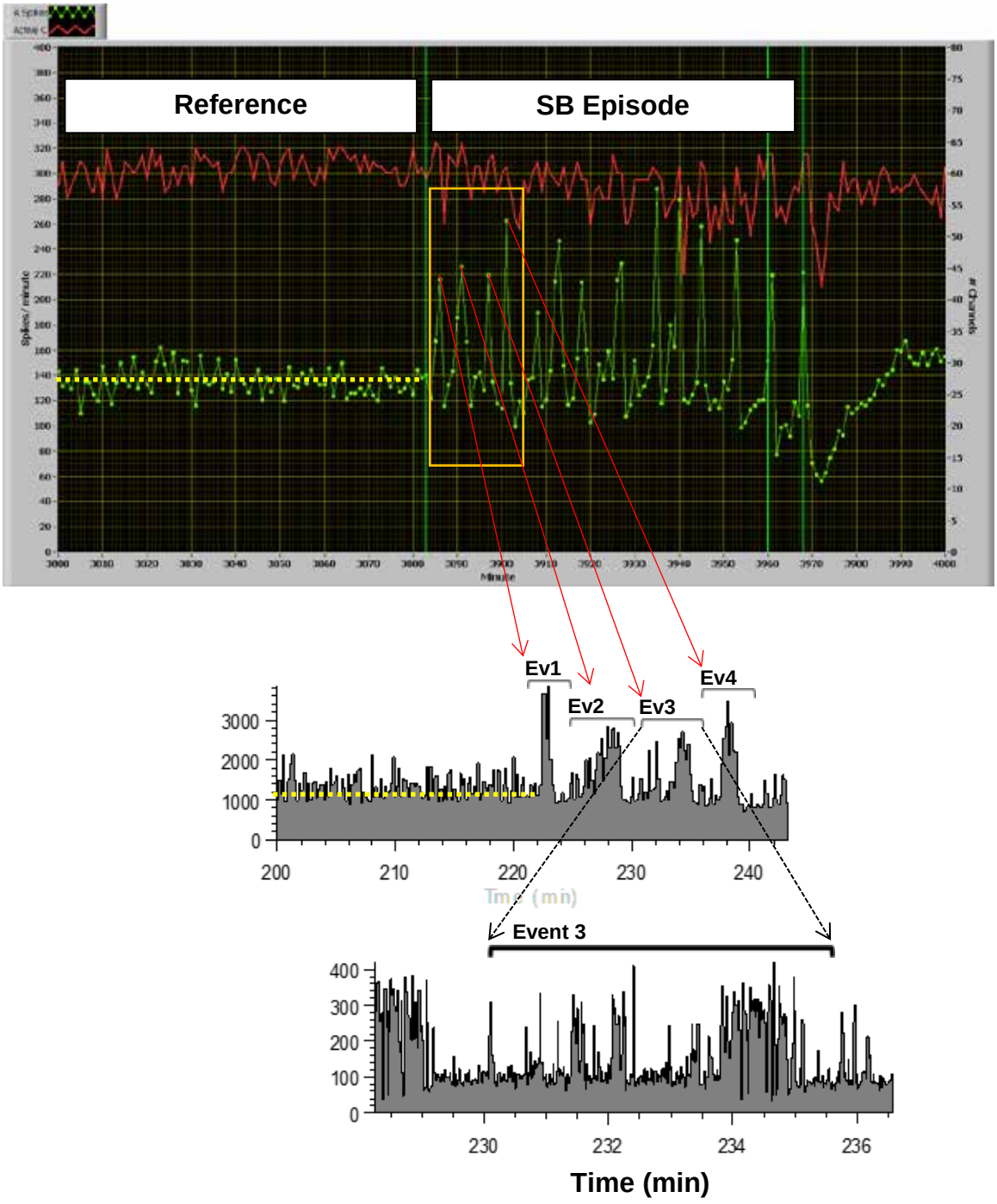

Fig. 14. SB fine structure in context. **(A)** VernAC experiment summary, featuring 4 SB events from 1 SB episode. **(B)** Increased resolution (decreased bin size) of previously featured 4 SB events, using total spike production (SB event #1-4, ~20 min., bin size= 10 sec.). **(C)** One SB event further increased in resolution to reveal a complicated SB fine structure (SB event #3, ~500 sec., bin size= 1 sec.).

4.3 SB Profile Quantification

4.3.1 Introduction of Phases

By increasing the activity profile resolution of a single SB event to reveal the fine structure (Fig. 14c), an interesting pattern was uncovered that can be divided into three “Phases” of varying length that are visually described in Fig. 15. Phase 1 (Ph. 1): a “build up” phase of increased coordinated bursting with an average 17.6% ± 13.7 (range: 3-42) increase in total spike production from reference activity; Phase 2 (Ph. 2): the “paroxysmal” phase, with a 52.9% ± 14.6 (range: 38-78) increase in total spike production from reference activity; Phase 3 (Ph.3): a “recovery” phase of lower coordination and an average 50.1% ± 35.6 (range: 8-96) decrease in total spike production from reference activity. In addition, corresponding 1d viewer data segments (NEX) also reveal pronounced activity phases (Fig. 15). All percent change data is calculated using total spike production and explained in more detail in the following section (4.3.2).

It is important to note that when comparing SB event phases with corresponding reference periods, data segment durations (the time base) must match. Normalizing the results provides for an accurate comparison of total spike production between reference and phase time periods. Inter-phase comparisons require a separate step of normalization accomplished by selecting a time base that matches the shortest SB event phase (Ph.1, 2, or 3) duration.

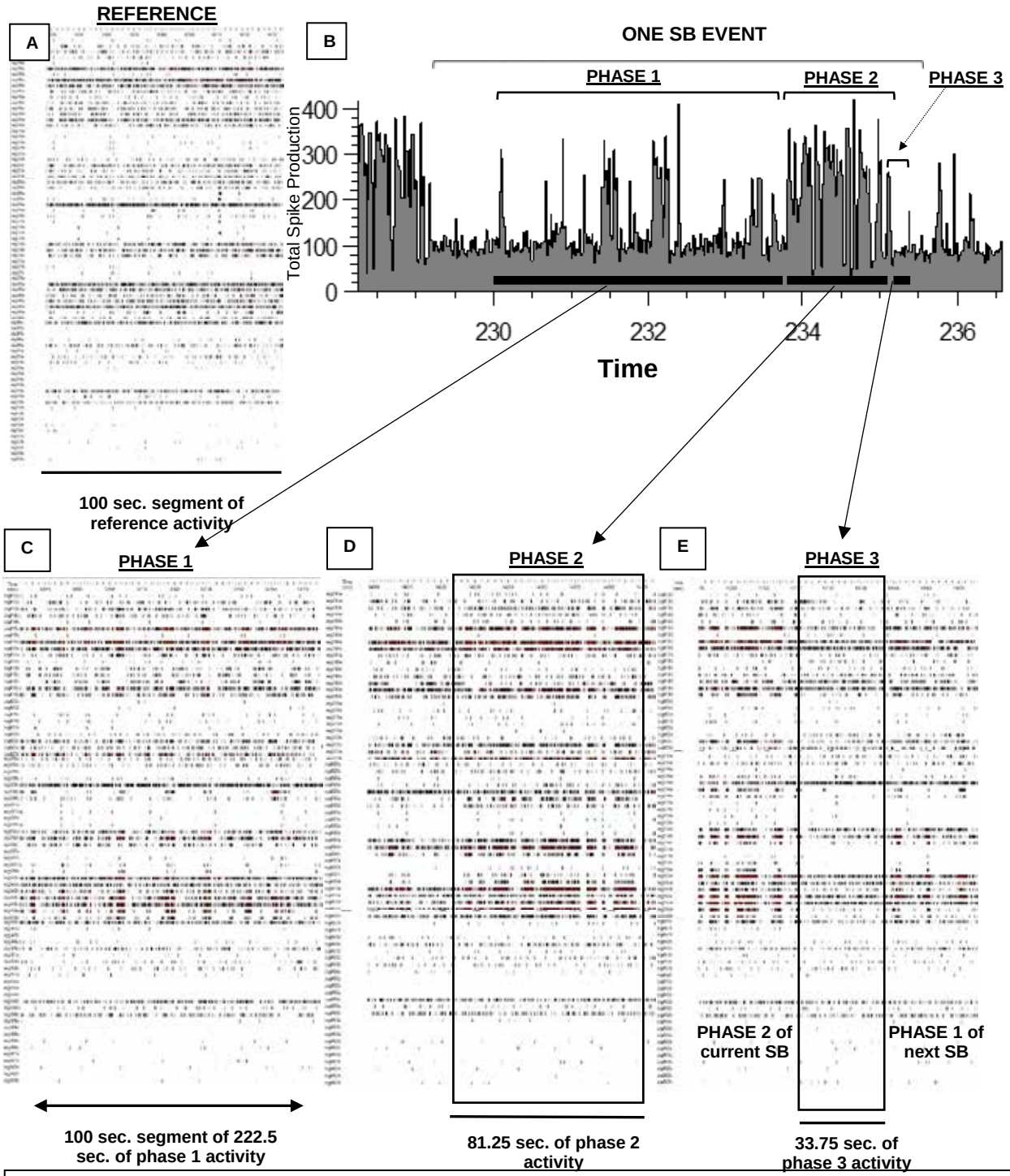

Fig. 15. Overview of SB Phases. **(A)** Reference activity visualized with NEX 1D viewer during a non-superbursting reference time period of 100 sec. (x-axis). Units are on the y-axis. **(B)** Fine structure overview (~8 min.) of a SB event with phases (Ph.1,2, and 3) identified using total spike production per minute (bin= 1 sec.). **(C,D, and E)** Ph. 1, 2, and 3 (respectively) NEX 1D viewer displays for comparison. Strengthened coordination relative to reference (A) is observed in Ph.1 (C) and Ph.2 (D) and can be visually determined by the increased grouping of vertical lines (activity).

4.3.2 Defining SB Phases with Total Spike Production

SB event phases were analyzed and defined using total network spike production. This approach used large fluctuations in spike activity to identify phase changes. Spike production was determined for Ph. 1, 2, and 3, and the corresponding relative reference periods, then normalized for comparison (Table 2). A significant difference ($p<0.001$) in total spike production was found between separate phases and corresponding relative reference periods. Relative reference periods did not reveal significant differences.

Large changes in spike production as compared to reference activity provide clear transitions between phases (Fig. 16). Fig. 16 compares total spike production for a single SB event and the corresponding reference period (bin= 1 sec.). Differences in profiles (spike production) are apparent and enlarged to show phases, which are identified using a two threshold identification method. For inter-phase comparison, total spike production for multiple phases from separate events is shown in Fig. 17 and summarized in Table 2. Briefly, increased coordinated bursting within the network can be seen in Ph. 1, with heavy spiking activity in Ph. 2 followed by a Ph. 3 activity reduction.

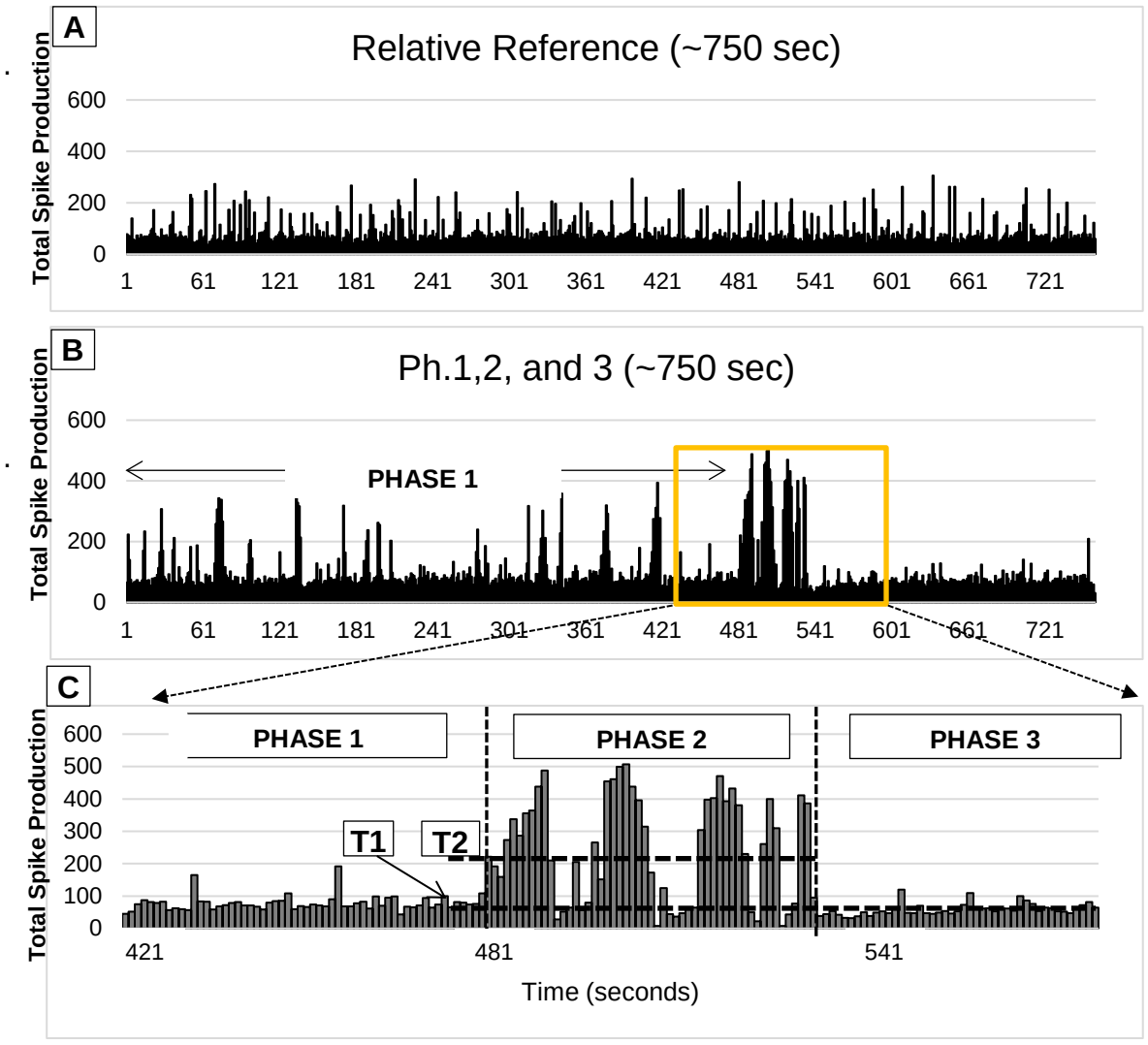

Fig. 16. Defining phases with changes in total spike production. **(A)** Total spike production over a ~750 sec. reference period. **(B)** SB Event (Phase 1,2, and 3) shown in corresponding time period (~750 sec., bin= 1 sec.) for total spike production (bin= 1 sec.). **(C)** Enlarged SB event with Phases 1, 2, and 3 identified. A two threshold system (two "T"s) was devised for integrated burst recognition to identify the beginning of Ph. 2. However, this is subject to "noise". Phase recognition is confirmed by a second threshold (T2) that is set for the following parameters: spike production must be at least 2x the preceding Ph. 1; duration must exceed 5 sec. Once a phase change is verified by T2, the T1 crossing is recorded as the starting point (vertical arrow). This system is currently executed manually, but should eventually be incorporated into a software design. While similar procedures may be possible for Ph. 1 and Ph. 3, it is beyond the scope of this thesis and must be the topic of a subsequent analysis.

Experiment #	SB Episode Number	SB Event Number	Phase 1 % Δ in spikes from reference	Phase 2 % Δ in spikes from reference	Phase 3 % Δ in spikes from reference
NS030/1/1	1	2	↑16%	↑66%	↓12%
NS030/1/2	1	3	↑26%	↑72%	↓8%
NS030/1/3	1	4	↑25%	↑68%	↓13%
NS030/2/1	2	2	↑10%	↑50%	↓22%
NS030/2/2	2	3	↑3%	↑40%	↓31%
NS030/2/3	2	4	↑20%	↑49%	↓39%
NS032/1/1	1	2	↑5%	↑57%	↓85%
NS032/1/2	1	3	↑5%	↑78%	↓94%
NS032/1/3	1	4	↑18%	↑57%	↓93%
NS032/2/1	2	2	↑42%	↑24%	↓84%
NS032/2/2	2	3	↑38%	↑38%	↓94%
NS032/2/3	2	4	↑37%	↑50%	↓96%
NS032/3/1	3	2	↑11%	↑42%	↓33%
NS032/3/2	3	3	↑10%	↑60%	↓16%
NS032/3/3	3	4	↑4%	↑42%	↓32%
		Average:	**+17.6%**	**+52.9%**	**-50.1%**
		SD:	**±13.7%**	**±14.6%**	**±35.6%**

Table 1. Summary of normalized changes in network activity during Ph. 1, 2, and 3 of multiple SB events. All measurements are based on comparisons to relative reference, as previously described. Current quantification methods are time consuming and labor intensive.

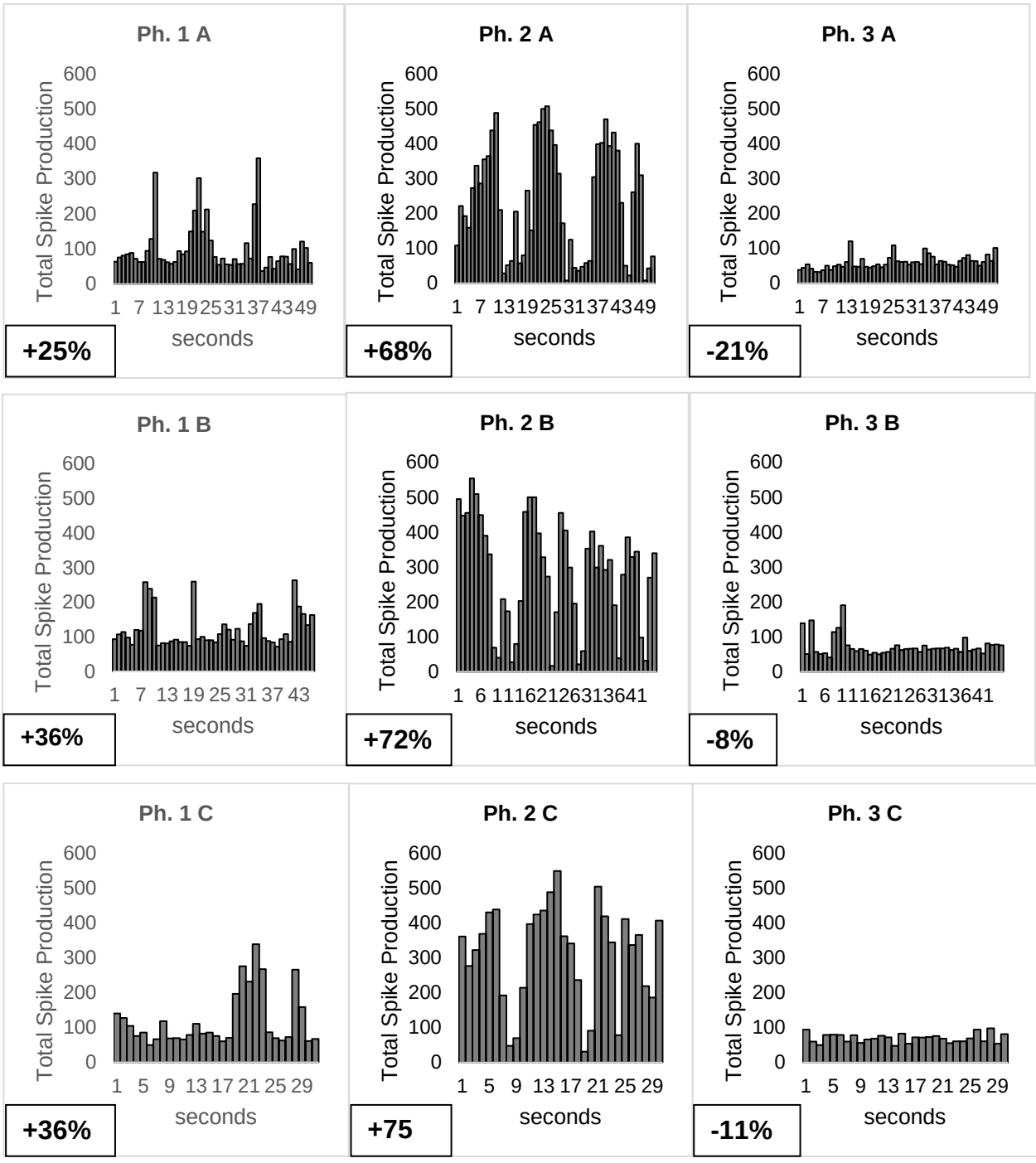

Fig. 17. Comparison of phases between 3 separate SB events (A, B, and C) using total spike production and percent change relative to reference. Columns: Phase 1, 2, and 3. Rows: Event A, B, and C. Corresponding percent activity changes are shown (boxed values) (bin= 1 sec.; summarized in Table 3 on the next page). Time bases are matched for inter-phase comparison (Row A: 50 sec; Row B: 45 sec; Row C: 30sec)

Event	Time Base	Ph. 1 Avg. Spikes	Ph. 2 Avg. Spikes	Ph. 3 Avg. Spikes	P1 % Δ	P2% Δ	P3 % Δ
A	50 sec	78.3	237.9	59.8	+25%	+68%	-21%
B	45 sec	113.9	285.5	72.6	+36%	+72%	-8%
C	30 sec	101.7	311.6	69.9	+36%	+75%	-11%

Table 2. Summary of data shown in Fig. 17. Inter-phase comparison between 3 separate SB events (A, B, and C). Normalized percent changes in activity are shown with their corresponding spike counts.

Defining SB phases with Coefficients of Variation

The coefficients of variation (CVs) can be used to determine the relative variability within a set of data (Gramowski et al., 2004). They are normalized standard deviations that allow comparisons of data sets with wide ranges of values. CVs can also be applied to quantify the degree of coordination of spike densities among active units during each phase. In multi-channel data sets, it is possible to investigate activity fluctuations in one minute or one second bins across all channels. Alternatively, it is also possible to observe fluctuations in a single unit over a specified time period and calculate resulting CVs for each unit. This approach to visualizing pattern fluctuations is shown in Fig. 18 and Fig. 19. Units (in this case specific waveshape-identified units) are arranged vertically, and time in terms of successive bins is represented by the horizontal axis. In this scheme, calculating CVs per bin across all units (vertically) reflects how well neuronal activity is coordinated in the network. The average of all such CVs over the experimental episode is called a CVnetwork (CVnw) (Keefer et al., 2001). The other pathway is the horizontal analysis where CVs are determined for a single unit across all bins for the activity episode of interest. Such a calculation shows the activity stability (or fluctuation) of a single unit in time. Large changes from bin to bin will be

reflected in a large CV. These CVs are averaged at the end of the episode for all active units to yield what has been called CVtime (CVtm). This scheme has been applied with some success to burst patterns (Gramowski et al., 2004), but is used here for the first time in an attempt to quantify spike density fluctuations

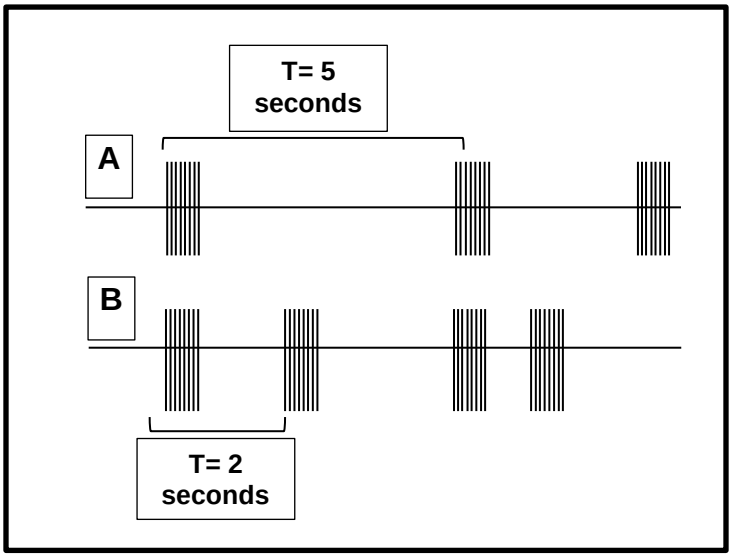

Fig. 18. Schematic explanation of CV utility. Two burst trains (A and B) have different burst periods and fluctuations. If the average period for A is 5 ± 1 sec. (SD) and for B 2 ± 1 sec., they would have the same standard deviation. However, the resulting CVs would be 20% and 50% respectively. The latter statistic often provides a better view of the degree of fluctuation in the burst period variable or any other selected variable such as number of spikes per bin.

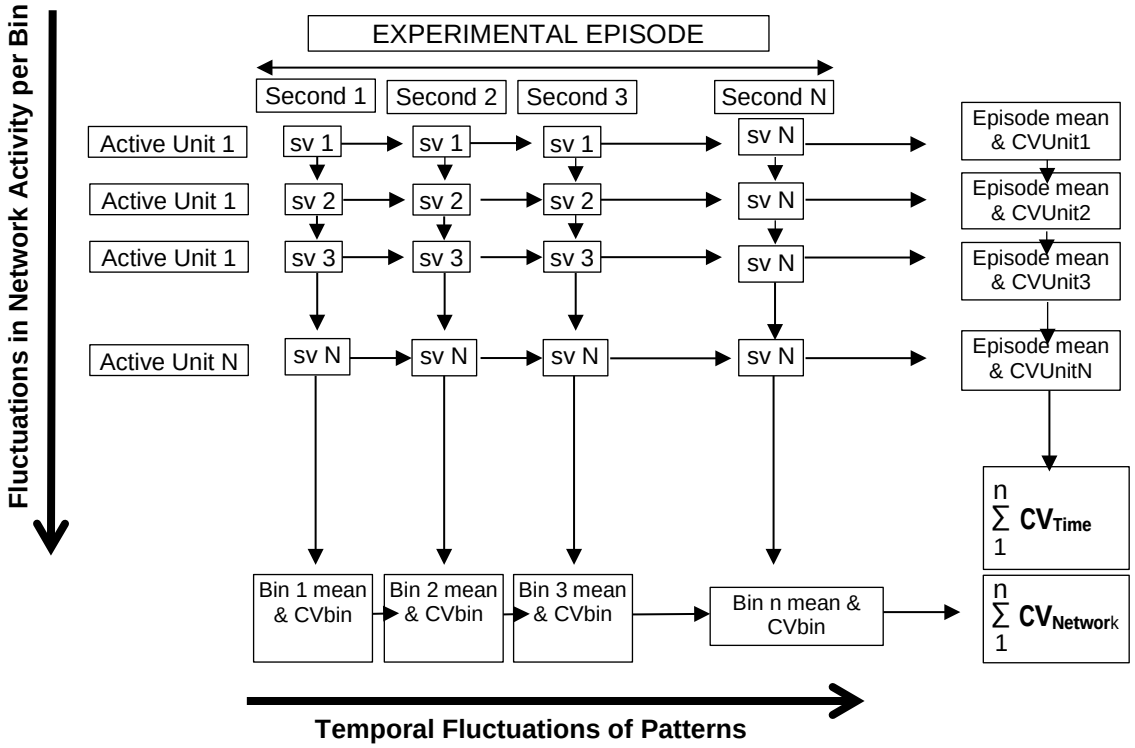

Fig. 19. Schematic of multichannel CV calculations. A vertical averaging in 1 sec. bins provides an average number of spikes from all units with an SD. This is converted to a CV for that particular bin. All such CVs are averaged for the entire selected time period, yielding a CVnetwork (CVnw). A low CVnw would imply good activity similarity among active units. The horizontal averaging provides a CV for each active unit. Averaging those for the data set provides a CVtime (CVtm). A low CVtm reflects a network that has a stable pattern in time. (*Adapted from Keefer et al., 2001).*

Ph. 2 CVnw and CVunit measurements are displayed in Fig. 20 with their corresponding relative references. A matching time base was determined by the length of the shortest data segment used (previously explained: in this example it was Ph. 2 with a 67 sec. duration). The unit CVs between reference and Ph. 2 vary considerably. While unit spike productions during reference are variable, Ph. 2 CVs are considerably similar. This reflects that high intensity spiking recruits most units into common activity patterns (greater coordination). Note that as the variability in spiking coordination within

the network is calculated over a period of time, the average of CVunit becomes CVtm (indicated as a red trace on the graph) and the average of CVbin becomes CVnw. A significant difference ($p = 0.0033$) in CVtm measurements was demonstrated between Ph. 2 and relative reference periods, while no such significance could be established for the CVnw (Fig. 20). As such, CVunit measurements are subsequently used. Additional CVs are shown in Fig. 21 for inter-phase comparison with similar results.

The simplest interpretation is that, despite large differences in spike production, the units (neurons) are tightly coupled but show, as a population, temporal activity (pattern) changes in the respective time segments. I conclude that, for identification of phases, the CV approach is less informative than the spike density plots shown in Fig. 17 and 16c. However, for experiments that involve synaptic damage or synaptic blockers, the CV calculations may show greater utility.

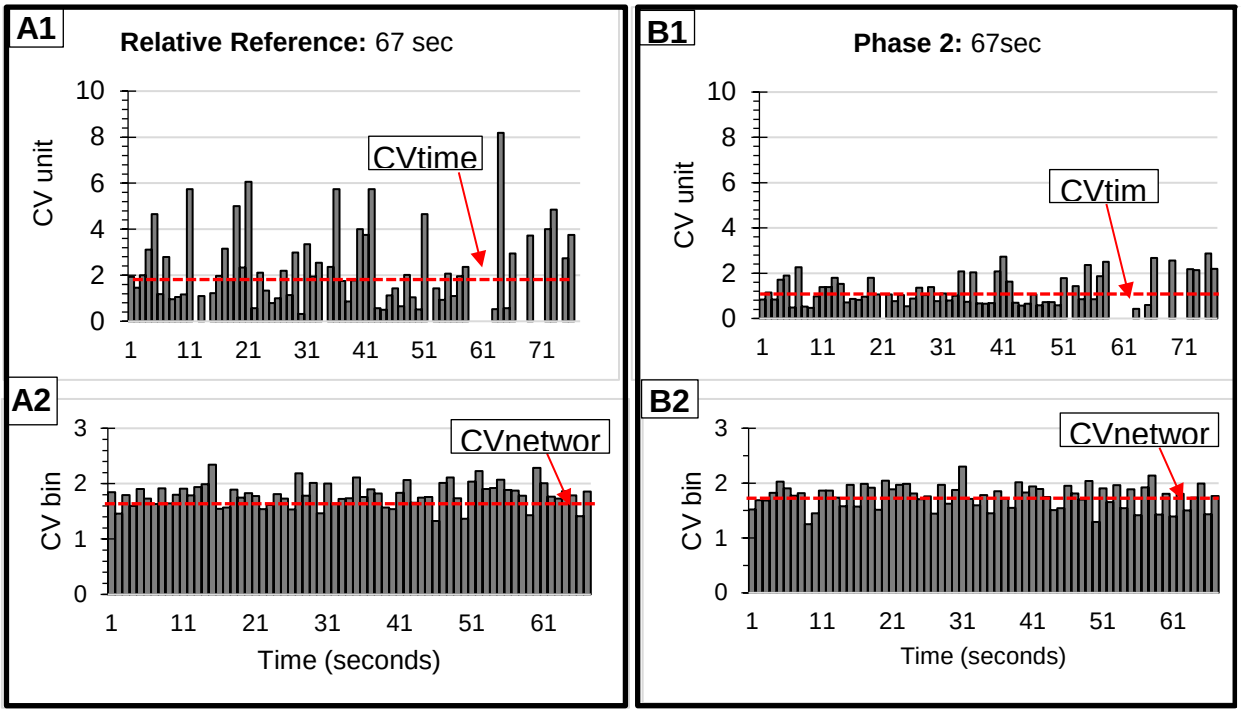

Fig. 20. Comparison of CVunit and CVnw measurements for reference (A1, 2) and Phase 2 (B1,2) (the paroxysmal phase) time periods. The graphs depict spike fluctuations (bin= 1 sec.) for all active units over a 76 sec. time period. **(A1)** The relative reference state shows greater spike production variability than what is found in Phase 2 (**B1**), even though the total spike production is much higher in Phase 2 (see Table 3). Average values of CVunit and CVnw for relative reference and Ph. 2 periods are 1.95 ± 1.78 and 1.27 ± 0.68 respectively (n= 72, p= 0.0033). **(A2 and B2)** Comparison of CV(nw) values during relative reference and Ph. 2 period. Despite a massive difference in spike production, channel to channel coordination across the entire network is almost the same and is reflected in similar CVnw values (A2 and B2). Average CVnw reference value: 1.80 ± 0.22; Average CVnw Ph. 2 value: 1.75 ± 0.22. (p= 0.181). Two tailed t test: GraphPad QuickCalcs

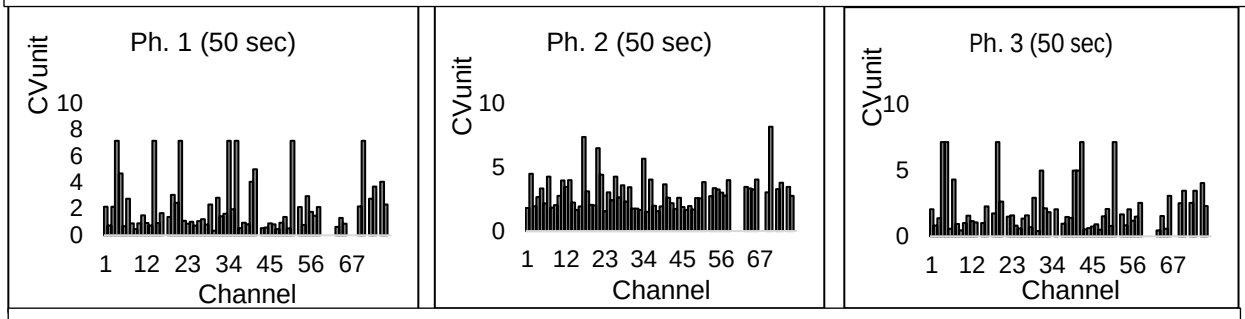

Fig. 21. Inter-phase comparison CVunit measurements. Consecutive Ph.1, 2, and 3 CVunit values are shown with a 50 sec. time base.

4.3.3 Comparing SB Phases: CVs and Total Spike Production

Combining separate approaches (CV and total spike production) to quantify SB event phases provided two unique views of SB fine structure. To determine if a correlation existed between activity increases (via total spike production) and enhanced coordination in units, CVunit and total spike production measurements were combined.

Two parameter “reflecting pool” graphs allowed for simultaneous visualization of two separate parameters (CV and spike density) for the same data set. The x axis for both parameters depicts pre-discriminated active units. The upper parameter shows total spike production in each active unit for a pre-selected time base (the corresponding phase length). Again, this time length is variable and depends on the length of the phase being analyzed. The lower parameter depicts the resulting CVunit value (the variability of spike production in individual active units for the length of the phase). These graphs are shown in Fig. 22 for each SB event phase with the corresponding relative reference activity.

Using two parameter reflecting pool graphs, Fig. 22 compares total spike production and CVunit for SB event Ph. 1,2 and 3, with corresponding reference periods. Again, a matching time base was selected for the respective phase and reference period. Whereas spike production is always in the upper segment of the graph, the lower segment can be either CVbin or CVunit. We have decided to show CVunit.

Total spike production for Ph. 1 occurred in slightly more dense packets (Fig. 22). However, Ph.1 CVunit remained relatively unchanged compared to reference. This indicates that there is not a drastic difference between Ph. 1 and the corresponding

reference time period (480 sec.).

Ph. 2 again shows a large increase in total spike production (Fig. 22). Differences in Ph. 2 CVunit values reveal an increase in unit spiking coordination compared to reference (56 sec.). It is important to remember that smaller CV values infer greater coordination.

A decrease in total spike production is again shown in Ph. 3 (Fig. 22). In addition, there also appears to be a slight increase in coordination within channels. The reference matched time period is 229 sec.

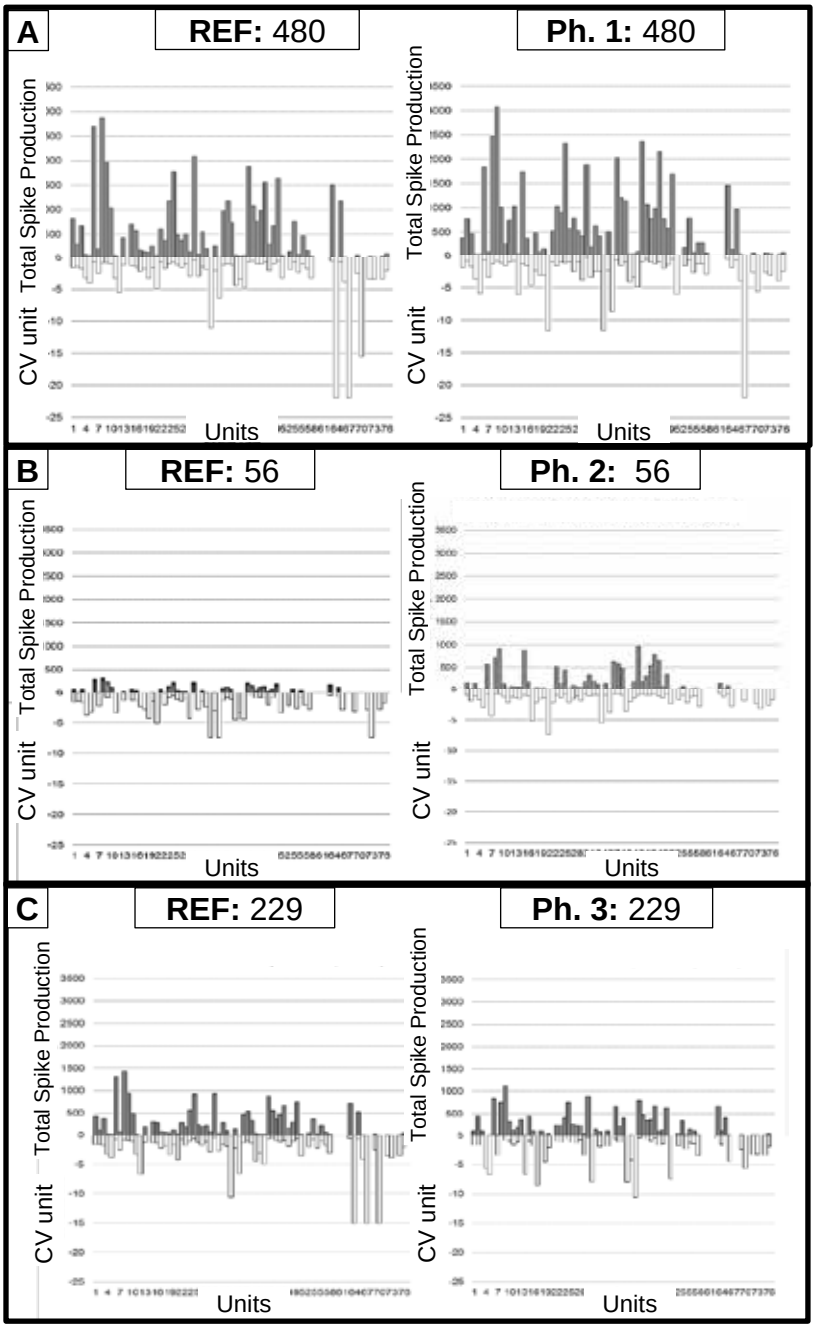

Fig. 22. Two parameter reflecting pool graphs for Ph. 1, 2, and 3, with matching relative reference periods (bin= 1 sec). It is important to remember that smaller CV values infer greater coordination.

(A) Ph. 1: 480 sec. of Ref. (left) and Ph. 1 (right) periods are compared using total spike production and CVunits.

(B) Ph. 2: 56 sec. of Ref. (left) and Ph. 2 (right) periods are compared using total spike production and CVunits.

(C) Ph. 3: 229 sec. of Ref. (left) and Ph. 3 (right) periods are compared using total spike production and CVunits.

The normalization of the y axes creates an artifact linked to the different time periods selected. This explains the low values in (B).

The largest CVs are always associated with periods of low spike density.

As previously mentioned, neither CVunit nor CVnw measurements produced results solely capable of consistently distinguishing separate SB phases. CVunit, the more distinguishing of the two, was selected for predominant use in figures and explanations. However, a brief summary of CVnw measurements is provided in Fig. 23. A reflecting pool graph was again selected to visualize both parameters (total spike production and CVnw), with time in seconds on the x axis. Even when examining the paroxysmal phase (Ph. 2: the most pronounced phase), CVnw values do not drastically differ from relative reference periods in spite of the substantial changes in spike production.

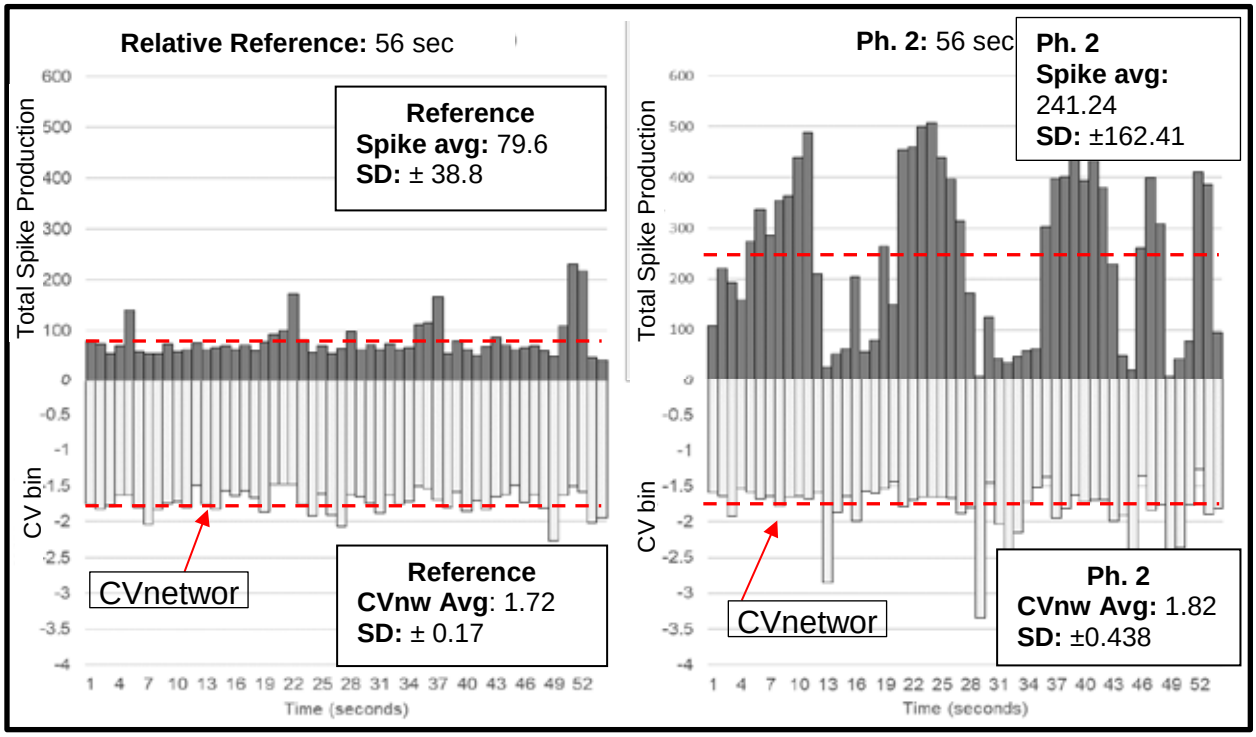

Fig. 23. Two parameter reflecting pool graphs (bin= 1). 56 sec. of relative reference (left) and Ph. 2 (right) periods compared using total spike production and CVnw. While total spiking activity between Ph. 2 and reference differs drastically (top), CVnw values do not (bottom: red line). Calculations (below) indicate that network coordination per sec in Ph. 2 and reference is relatively comparable.

4.4 Controlling SB Activity

4.4.1 SB Induction by Osmotic Shock

Through osmotic shock inductions, by rapidly (immediately) introducing either a hyper-osmotic or hypo-osmotic solution to the already equilibrated medium of a culture, SBs were found to be inducible (osmo-induced SBs). Generally, hyper-osmotic SB inductions (range: 300-340 mOsm.) dampened network activity almost entirely, with less frequent and less pronounced SBs emerging much later (~2 hrs.). Hypo-osmotic inductions (range: 270-300 mOsm.) featured almost immediate fluctuations in activity, resulting in SBs soon (~20 min.) after. Both hypo and hyper osmotically affected networks typically attained higher baseline activity levels post osmotic shock as compared to relative reference.

A hypo-osmotic induced SB episode is described and compared with a native SB profile in Fig. 24. While general SB profile structure was consistent, osmo-induced SB event durations generally lasted much longer (~8x) than native SB events (Table 4). In addition, native SBs appeared to be much more sporadic in terms of activity (Ph. 1, Fig. 24B), with large changes in overall spike production occurring more frequently than in osmo-induced SB.

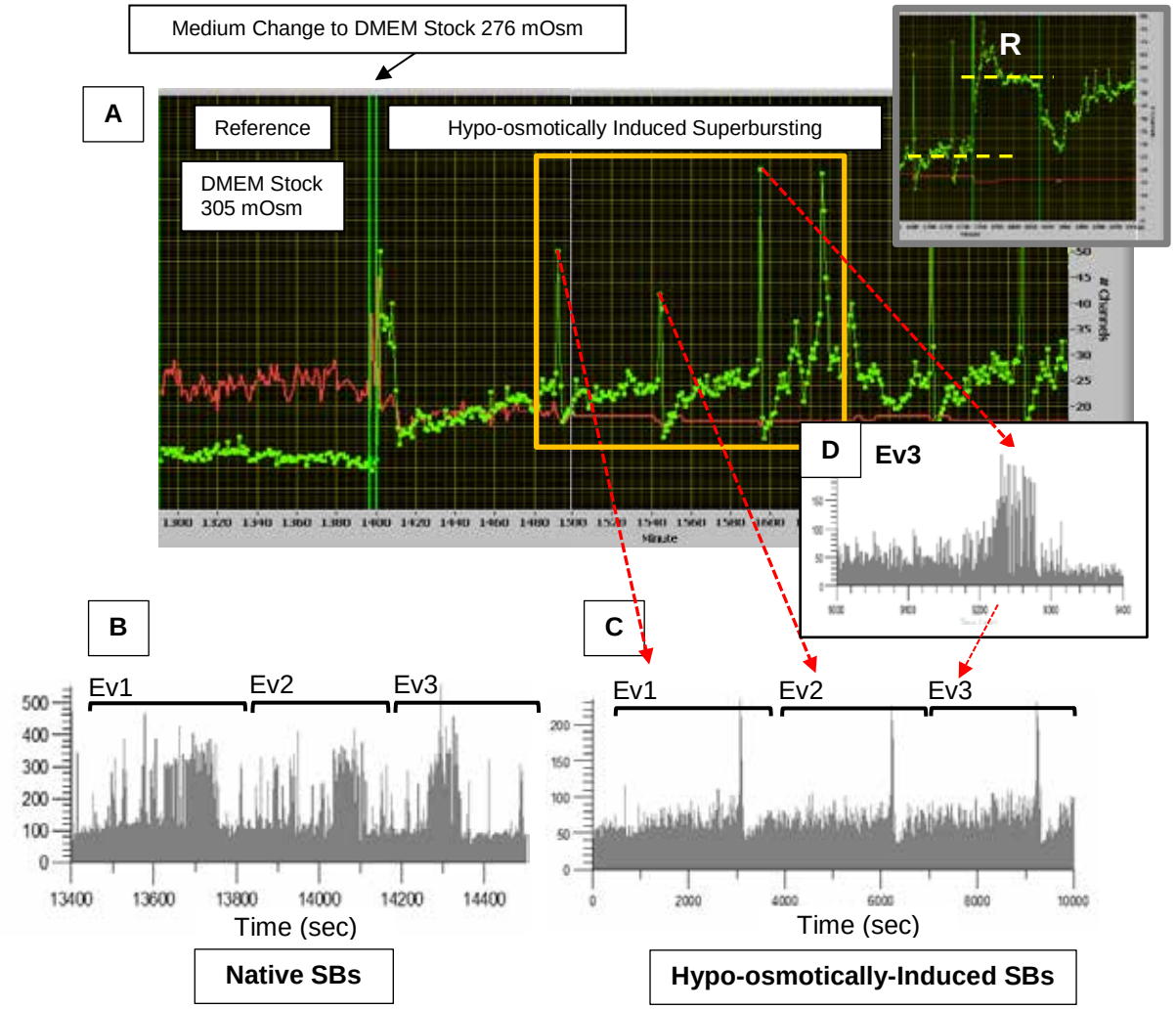

Fig. 24. (A) Overview of osmotically induced SB profiles. Top right insert: example of increased reference activity baseline (R) post osmotic shock. **(B)** Profiles (total spike production) for the 3 corresponding events in (A). **(C)** A separate spontaneously SB (native SB) experiment, featuring total spike production profiles also for 3 consecutive events, for comparison. It is interesting to note, that while some similarities are apparent between native SB and osmo-induced SB profiles, event durations differ drastically. Osmo-induced SB event durations are almost ~8x longer than corresponding native SB events. Bin: 1 sec. **(D)** Expansion of event 3 to the same time scale as B.

Exp. #	Initial Osmo (mOsm)	Final Osmo (mOsm)	Event	Event Duration (sec)	Ph. 1 Duration (sec)	Ph. 2 Duration (sec)	Ph. 3 Duration (sec)
NS072	305	276	1	1552.5	1460	71	21.5
			2	2610	2550	53	7
			3	2723.5	2657.5	58	8

Table 3. Summary of osmo-induced SB phase durations from Fig. 24.

4.4.2 SB Control with Medium Flow

Experimental evidence has shown that medium circulation stabilizes network activity. To allow systematic studies of these early observations, existing flow chambers were coupled with a peristaltic pump to circulate medium (as described in methods). Through the introduction of medium movement via a peristaltic pump, spontaneous SB activity ceased in a somewhat delayed (mean: 28.3 min. ±7.6, n= 17) manner (Fig. 25). Stable network activity remained for up to ~24 hr. Table 4 depicts the time between the onset of medium flow movement and the complete stabilization of network activity. However, pump cessation resulted in an almost instantaneous (mean: 8.5 min., n= 11) return of superbursting activity (Fig. 26) and is summarized in Table 5. In addition, osmotic shock induced SBs (from previous section) were also suppressed by gentle medium agitation, with superbursting activity reemerging after pump cessation.

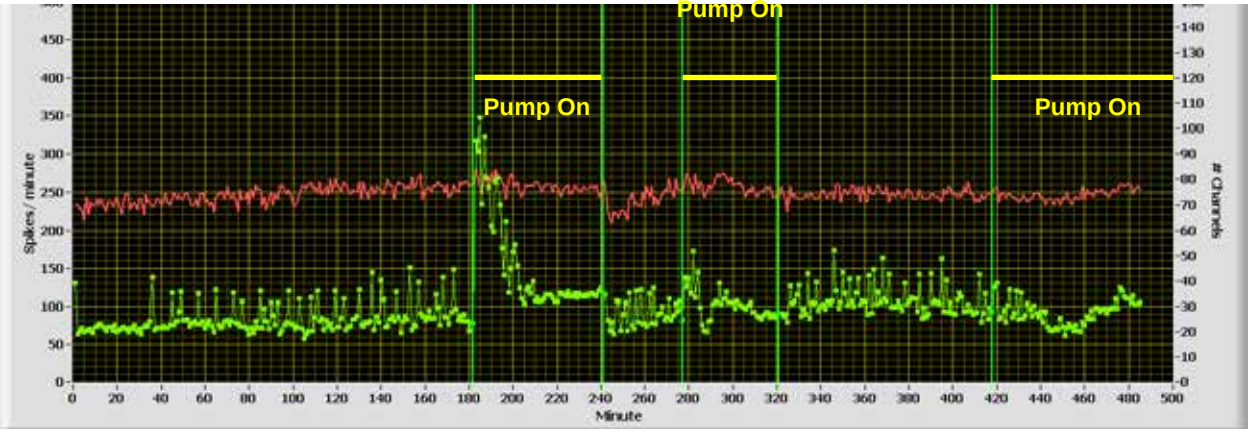

Fig. 25. Controlling SBs with peristaltic pump activation: Successive cycles of medium flow via pump activation/deactivation in experiment NS030 from 0 - 500 min. Activity stabilization is achieved with pump activation and is identified with yellow bars

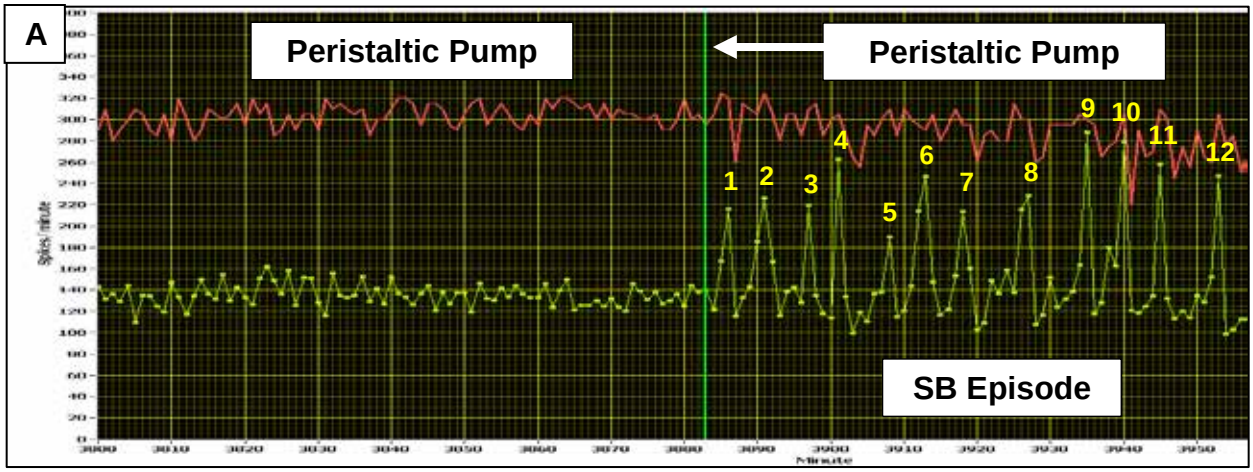

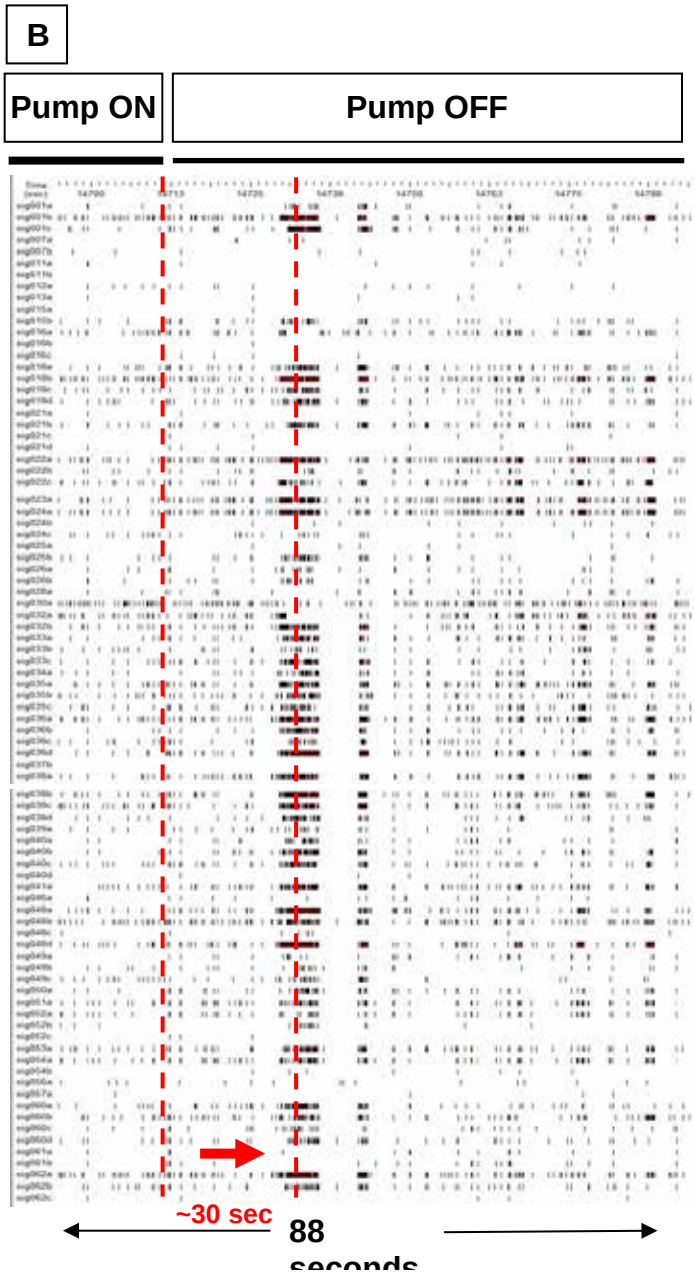

Fig. 26. Overview of a SB episode initiation resulting from pump cessation. **(A)** Transition from stable activity under constant flow of medium (pump on) to a SB episode (12 events) after pump cessation. **(B)** Sudden onset of Ph. 1 burst packets rapidly (30-40 sec.) following the halt of medium flow (pump deactivation). Ph. 2 does not start until ~2 min. later and is not shown.

Experiment ID-cycle #	Time between start of peristaltic flow and activity
NS030-1	42 min.
NS030-2	32 min.
NS030-3	27 min.
NS030-4	24 min.
NS030-5	26 min.
NS030-6	35 min.
NS031-1	29 min.
NS031-2	29 min.
NS032-1	28 min.
NS032-2	21 min.
NS032-3	25 min.
NS032-4	17 min.
NS032-5	20 min.
NS032-6	30 min.
NS032-7	40 min.
NS032-8	41 min.
NS040-1	16 min.
Average:	**28.3 min**
Standard Deviation:	**7.8 min**
n:	**17**

Table 4. Minutes required for network stability after pump introduction for multiple SB episodes in separate experiments.
It is interesting to note that network stability is not immediately achieved after the introduction of a peristaltic pump into the flow system. This activity stabilization requires 28.3 min. on average from the onset of medium movement.

Experiment ID- Cycle #	Time between cessation of pump and first SB occurrence (min)
NS030-1	1 min.
NS030-2	1 min.
NS030-3	1 min.
NS030-4	1 min.
NS032-1	5 min.
NS032-2	4 min.
NS032-3	9 min.
NS032-4	18 min.
NS032-5	21 min.
NS032-6	15 min.
NS032-7	18 min.
NS040-1	16 min.
Average:	**9.2 min**
Standard Deviation:	**7.9 min**
n:	**11**

Table 5. Minutes until SB episode initiation after pump cessation for multiple SB episodes in separate experiments. Superbursting activity occurs almost immediately after the pump has been shut off and flow has been stopped.

4.4.3 SB Control with Medium Flow at Varying Pump Rates

Multiple peristaltic pump settings were investigated in an attempt to correlate flow rates with changes in activity. Pump parameters are divided into values ranging from 0 – 100, representing minimum and maximum values in arbitrary units. Four separate values (10, 25, 30, and 90) were selected and tested on superbursting networks. The results are summarized in Fig. 27 and 28. An approximate threshold of pump effectiveness for controlling superbursting activity appeared at 10, or ~ 0.04 ml/min. Lower settings were only temporarily effective and resulted in the eventual reappearance of SBs. Higher pump settings (90, or ~0.4 ml/min) provided indefinite (up to ~24 hr) SB suppression (Fig. 27).

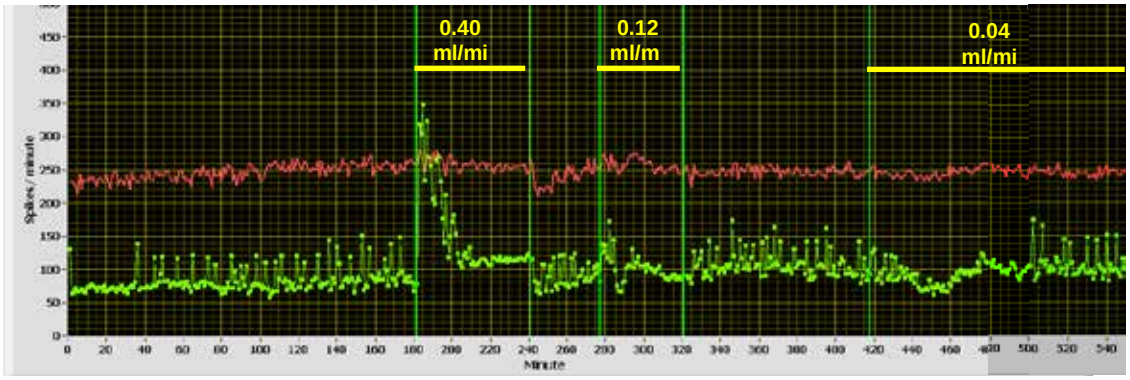

Fig. 27. Varying peristaltic pump speeds and the resulting suppression effects on network activity. With a constant medium flow rate of 0.40 ml/min, network activity is stabilized over time (mean: 28.3 min.) indefinitely (max: 24 hr). In addition, a flow rate of 0.12 ml/min resulted in a similar pattern of activity. However, a flow rate of 0.04 ml/min appears to only temporarily subdue SB activity. While activity seems to stabilize, slower oscillations are seen and eventually superbursting behavior develops. The large response at 180 min. may be an artefact of media pH (fresh media not bing)

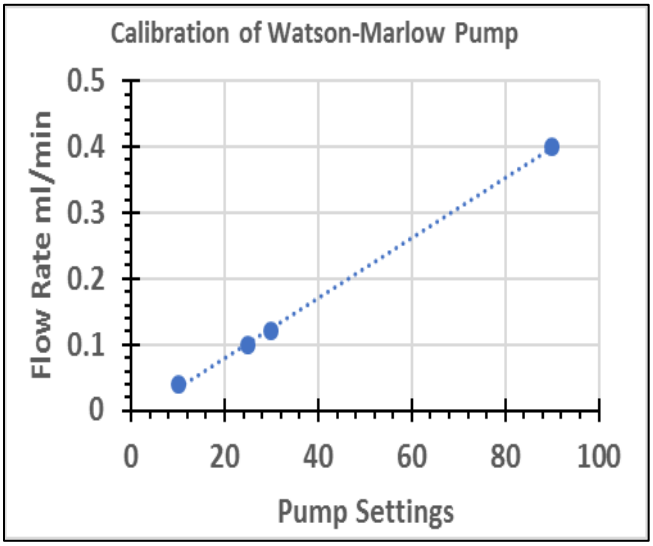

Fig. 28. Peristaltic pump settings matched with flow rates graphed as a calibration curve.

Pharmed tubing:
inner diameter: 1 mm
outer diameter: 3 mm

CHAPTER 5

DISCUSSION

This thesis was conducted to further understand the features and underlying mechanisms of SBs. Qualitative and quantitative definitions for SB fine structures were devised to better analyze and explain this complex phenomenon. Through manipulations of medium flow with a peristaltic pump, native SBs were suppressible, while cessation of medium flow resulted in the reemergence of SBs. Additionally, by manipulating the medium environment of a culture, through osmotic shock, we found the superbursting phenomenon to be also inducible.

SBs can be described as spontaneous, high intensity coordinated burst oscillations which self-terminate. However, the major oscillations can last for very long times and contain numerous high intensity discharges. What separates superbursting from normal population bursts in networks, including those generated via disinhibition with 40 μM bicuculline, are the intense and long-lasting oscillations of bursts. At a resolution of 1 min, the oscillations appear as major increases in network spike production, lasting on average 4.4 ± 1.2 minutes (range: 3-6) when activity decays back to reference. I have termed this ~4 minute increase in spiking activity an “SB Event”. These events appear as long lasting, major oscillations that I have called an “SB Episode”. Since SB Episodes were manipulated by the experimenter through utilization of a peristaltic pump, data regarding the average range of SB events produced by a culture for one SB episode is unknown.

Within one SB event, a fine burst packet structure emerges. Qualitative analyses revealed each SB event can be described in terms of three distinct phases. Phase 1

(Ph. 1) consists of random, coordinated bursting within the network. Phase 2 (Ph. 2) is comprised of highly coordinated, intense spiking forming variable, but dense burst packets lasting ~1 minute. The following phase 3 (Ph. 3) typically exhibits a decrease in spiking activity and bursting.

A two-threshold system was devised to define phase changes in terms of total spike production to identify the beginning of Ph. 2. Once an initial increase in total spike production threshold is crossed (T1), a second threshold (T2) consisting of at least a 2x increase in total spike production exceeding 5 seconds must be met. After T2 parameters have be met, T1 crossing may be recorded as the starting point. This process was manually utilized in determining phase changes. Upon further quantitative analyses of phases, a range of percent changes for each phase compared to a relative reference was calculated. Relative references were calculated by averaging total unit spike production from three reference segments, from the period preceding the SB episode of interest. This reference was used for calculating percent changes in total active unit spiking activity during each phase. Compared to this reference, Ph. 1 was found to have a 5-42% increase in total spike activity, Ph. 2 consists of a 38-72% increase in total spike activity, and Ph. 3 exhibited an 8-96% decrease in total spike activity. These three distinguishable phases may be useful in further analyzing the SB event structures resulting from other SB induction methods.

Coefficients of variation were calculated to quantify phase transitions. While CVunit showed interesting trends in the spiking coordination of one unit over a designated period of time between phases, resulting CV network (CVnw) calculations were much less informative. When analyzing CVunit of Ph. 2 activity, a much higher

degree of coordination (low CV) within unit spiking was shown in comparison to reference activity, indicating that each unit experiences less spiking variability during Ph. 2 than during reference. CVnw values alone were not capable of distinguishing between different phases, and thus were not helpful. They do, however, show a similar level of spiking coordination within the network regardless of phase.

Some mechanisms may now be suggested- one specifically dealing with accumulation of potassium (K+) ions. Under stagnant conditions, normal bursting increases external potassium concentration in enrichment layers immediately above and below the cells. This causes a positive feedback loop by decreasing membrane potential magnitude bringing cells closer to threshold and triggering a paroxysmal global discharge. The phenomenon is most likely greatly enhanced in highly dense cultures.

To verify whether potassium concentrations increase extracellularly, it is possible to use an indirect method to at least correlate superbursting with increasing external potassium ions. This method uses action potentials recorded during a reference period and during superbursting. I have compared action potential amplitudes derived from those two time periods (Fig. 29). It can be seen that there is a decrease in amplitude (13-20%). Such decreases can be caused by the relative refractory period, which is spike frequency-dependent, or by the accumulation of external potassium. These observations do not prove the involvement of potassium ions. However, spike frequencies do not greatly differ between reference and the SB event (Fig. 29), which makes the potassium ions the better explanation. If the layer of increased potassium is not removed by glia and/or by circulation, the associated reduction in membrane potentials can enhance excitation that would result in intense bursting.

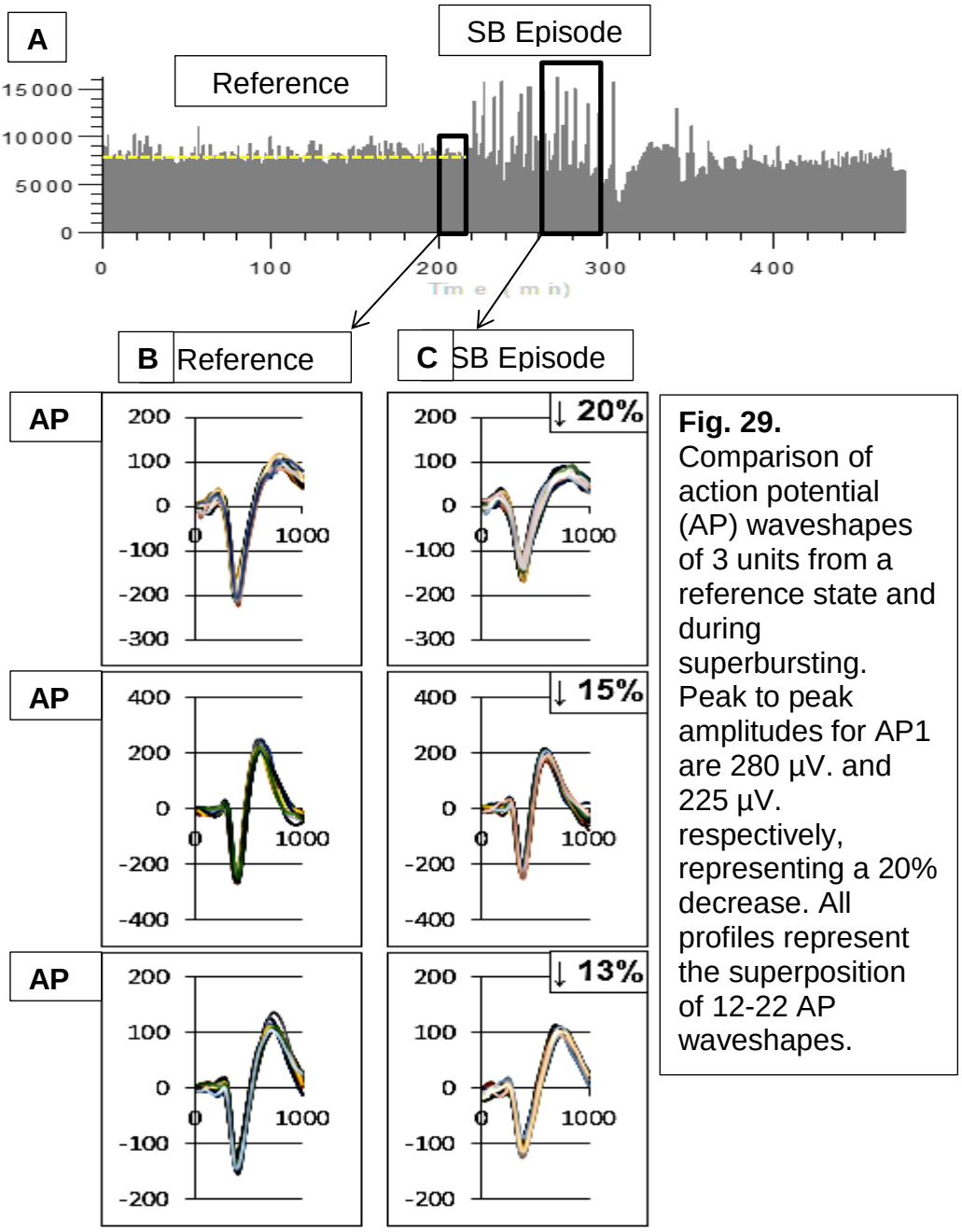

Fig. 29. Comparison of action potential (AP) waveshapes of 3 units from a reference state and during superbursting. Peak to peak amplitudes for AP1 are 280 µV. and 225 µV. respectively, representing a 20% decrease. All profiles represent the superposition of 12-22 AP waveshapes.

Loss of potassium regulation has a linkage to epileptiform activity *in vivo*, and several studies have linked this similar network behavior *in vitro* (Spain et al., 1987; Jensen and Yaari, 1997; Pan and Stringer, 1997). Additions of KCl to a network, have been shown to increase burst rate in networks *in vitro* utilizing our methodologies (see Fig. 30) (Keefer et al., 2001). Similar irregularities in activity, or paroxysmal superbursting behavior, was demonstrated in section 4.4 and was shown to be influenced by medium flow manipulations. Once flow was introduced, cessation of superbursting activity took an average of 28.3 ± 7.8 minutes (range: 16-42). However, once the flow was terminated superbursts typically reappeared in approximately 9.2 ± 7.9 minutes (range: 1–21). Since networks *in vitro* lack circulation, the termination of SBs could be a result of the removal of any potential stratification around cells by medium flow. In this case, the medium flow is essentially serving as a circulatory system by removing build-up of ions and metabolic waste products. Due to the high volume of cells in some cultures, this “cleansing” process could take time thus resulting in a longer time period to activity stabilization and superburst cessation. Conversely, the rapid re-appearance of SBs in ~9 minutes reflects increases in K+ ion concentrations from residual activity in the network. It could be that these neurons are bursting at sufficiently high rates to create a stratification layer.

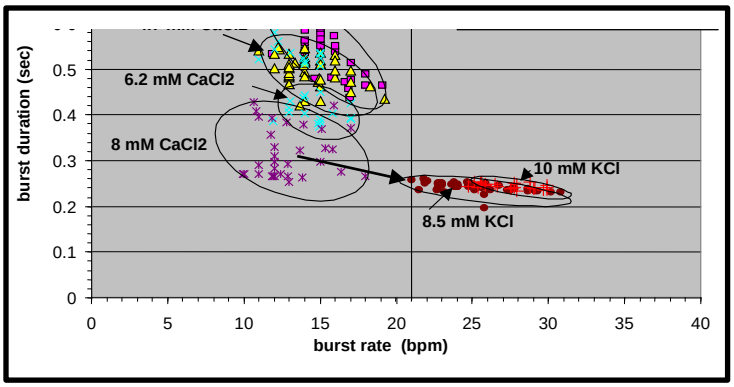

Fig. 30. Network state graph obtained by plotting burst rate against burst duration. A KCl concentration change from the normal 3 mM to 8.5 mM increased the burst rate from 13 to 22 bpm (large arrow). A further increase to 10 mM accelerated the burst rate to a maximum 30 bpm. Redrawn from Keefer et al., 2001.

Additionally, with the immediate introduction of hyper-/hypo-osmotic solutions, I was able to induce superbursting in cultures. When comparing native SB phase structure to the osmotically induced SBs, there is a clear difference between the two possibly indicating that differing underlying mechanisms could be affected resulting in this abnormal bursting behavior. While osmotic manipulations were found to induce superbursting, a recent study has found that through the treatment of hippocampal brain slices with hyaluronidase, superbursting activity was inducible (Vendunova et al., 2013). This indicates other SB induction methods are possible and should be explored.

The SB high frequency oscillatory patterns self-terminate. This may be linked to the exhaustion of vesicles in the readily releasable pool of synapses (Keefer et al., 2001; Stevens et al., 1995). These oscillatory patterns underlying similar paroxysmal bursting activity have also been identified *in vivo*. By increasing extracellular potassium, the network is triggered to shift from an awake-state of oscillatory behavior to seizure-like oscillations (Bazhenov et al., 2004).

Many different factors appear to cause epileptiform activity. They range from loss or inactivation of inhibitory neurons in the focal area, to excessive sprouting of excitatory

fibers, ion channel dysfunction, and also sensory-induced oscillations (Chang and Lowenstein, 2003). It is conceivable that local loss or blockage of capillaries can lead to diffusion-limited processes that may involve an interplay of lactate and ammonium ion activity inhibition and K+ concentration-dependent excitation. Such a mechanism would come close to what is observed so far *in vitro*.

While SBs are epileptiform in nature, reliable links between SBs and epilepsy cannot currently be made. Since the research of hypothesized mechanisms involved in epilepsy is so vast, careful scrutiny of literature must first be made. Additionally, epilepsy *in vivo* is primarily analyzed by EEGs rather than using spike patterns making direct comparisons difficult. Although further analyses must be completed in order to make these concrete relationships, there is still a dynamical similarity between the two phenomena.

Future analyses utilizing our methodologies should include investigating alternate SB inductions and control over the fine structure of SB events. If Ph. 1, the slow buildup of activity, can be quantitatively identified it may be possible to prevent the development of the paroxysmal Ph. 2 via electrical stimulation. Further, by analyzing, defining, and manipulating superbursts, we can provide a quantitative linkage to epileptiform activity.

REFERENCES

Bazhenov, M., Timofeev, I., Steriade, M., & Sejnowski, T. J. (2004). Potassium model for slow (2-3 Hz) in vivo neocortical paroxysmal oscillations. *Journal of neurophysiology*, *92*(2), 1116-1132.

Chang SB, Lowenstein DH (2003) Epilepsy. N Engl J Med 349: 1257-1266.

Chiappalone, M., Vato, A., Berdondini, L., Koudelka-Hep, M., & Martinoia, S. (2007). Network dynamics and synchronous activity in cultured cortical neurons. *International journal of neural systems*, *17*(02), 87-103.

Gladkov, A., Grinchuk, O., Pigareva, Y., Mukhina, I., Kazantsev, V., & Pimashkin, A. (2018). Theta rhythm-like bidirectional cycling dynamics of living neuronal networks in vitro. *PloS one*, *13*(2), e0192468.

Gramowski, A., JuÈgelt, K., Weiss, D. G., & Gross, G. W. (2004). Substance identification by quantitative characterization of oscillatory activity in murine spinal cord networks on microelectrode arrays. *European Journal of Neuroscience*, *19*(10), 2815-2825.

Gross GW (2011) Multielectrode Arrays. Scholarpedia, 6(3): 5749

Gross, G.W. and Schwalm, F.U. (1994) A closed chamber for long-term electrophysiological and microscopical monitoring of monolayer neuronal networks. J. Neuroscience Methods 52: 73-85.

Gross, G.W., Wen, W. and Lin, J. (l985). Transparent indium-tin oxide patterns for extracellular, multisite recording in neuronal cultures. J. Neurosci. Meth. 15: 243-252.

Idelson, M. S., Ben-Jacob, E., & Hanein, Y. (2010). Innate synchronous oscillations in freely-organized small neuronal circuits. *PloS one*, *5*(12), e14443.

Jensen, M. S., & Yaari, Y. (1997). Role of intrinsic burst firing, potassium accumulation, and electrical coupling in the elevated potassium model of hippocampal epilepsy. *Journal of neurophysiology*, *77*(3), 1224-1233.

Keefer, E.W., Gramowski, A., and Gross, G.W. (2001) NMDA receptor dependent periodic oscillations in cultured spinal cord networks. J. Neurophysiol. 86: 3030-3042.

Kim, J. H., Heo, R., Choi, J. H., & Lee, K. J. (2014). Dynamic transitions among multiple oscillators of synchronized bursts in cultured neural networks. *Journal of Statistical Mechanics: Theory and Experiment*, *2014*(4), P04019.

Kowalski, J.M., Albert, G.L., Rhoades, B.K., and Gross, G.W. (1992) Neuronal networks with spontaneous, correlated bursting activity: theory and simulations. Neural Networks 5: 805- 822.

Krahe R, Gabbiani F (2004) Burst firing in sensory systems. Nature Reviews Neuroscience 5, 13-23 (January 2004

Madhavan, R., Chao, Z. C., & Potter, S. M. (2007). Plasticity of recurring spatiotemporal activity patterns in cortical networks. *Physical biology*, *4*(3), 181.

Meyer, J.M., Wolf, B., and Gross, G.W. (2009) Magnetic stimulation and depression of mammalian networks in primary neuronal cell cultures. IEEE Biomedical Engineering. Vol 56, No.5, 1-12.

Morefield, S. I., Keefer, E.W., Chapman, K. D., and Gross, G.W. (2000) Drug evaluations using neuronal networks cultured on microelectrode arrays. Biosensors and Bioelectronics 15:383-396.

Pan, E., & Stringer, J. L. (1997). Role of potassium and calcium in the generation of cellular bursts in the dentate gyrus. *Journal of neurophysiology*, *77*(5), 2293-2299.

Ransom, B. R., Nelson, P. G., Henkart, M., & Bullock, P. N. (1977). Mouse spinal cord in cell culture. IV. Modulation of inhibitory synaptic function. *Journal of Neurophysiology*, *40*(5), 1178-1187.

Segev, R., Benveniste, M., Shapira, Y., & Ben-Jacob, E. (2003). Formation of electrically active clusterized neural networks. *Physical review letters*, *90*(16), 168101.

Spain, W. J., Schwindt, P. C., & Crill, W. E. (1987). Anomalous rectification in neurons from cat sensorimotor cortex in vitro. *Journal of neurophysiology*, *57*(5), 1555-1576.

Stevens, C. F., & Tsujimoto, T. (1995). Estimates for the pool size of releasable quanta at a single central synapse and for the time required to refill the pool. *Proceedings of the National Academy of Sciences*, *92*(3), 846-849.

Vedunova, M., Sakharnova, T., Mitroshina, E., Perminova, M., Zakharov, Y., Pimashkin, A., & Mukhina, I. (2013). Seizure-like activity in hyaluronidase-treated dissociated hippocampal cultures. *Frontiers in cellular neuroscience*, *7*, 149.

Wagenaar DA, Madhavan R, Pine J, Potter SM (2005) Controlling bursting in cortical cultures with closed-loop multi-electrode stimulation. J Neurosci. 25 (3): 680-688.

Wagenaar, D. A., Nadasdy, Z., & Potter, S. M. (2006). Persistent dynamic attractors in activity patterns of cultured neuronal networks. *Physical Review E*, *73*(5), 051907.

Wagenaar, DA, Pine J, Potter SM (2006) An extremely rich repertoire of bursting patterns during the development of cortical cultures. BMC Neurosci 7: 11. doi:10.1186/1471-2202-7-11.

Wagenaar, D. A. (2006). *Development and control of epileptiform bursting in dissociated cortical cultures* (Doctoral dissertation, California Institute of Technology).

Wu C, Gopal KG, Gross GW, Lukas JT, Moore EJ (2011) An *in vitro* model for testing drugs to treat tinnitus. European Journal of Pharmacology. DOI: 10.1016/j.ejphar.2011.05.070